ADVANCED MATERIALS
www.advmat.de

Design Criteria for Nanostructured Carbon Materials as Solid Contacts for Ion-Selective Sensors

Yevedzo E. Chipangura, Brian D. Spindler, Philippe Bühlmann, and Andreas Stein**

The ability to miniaturize ion-selective sensors that enable microsensor arrays and wearable sensor patches for ion detection in environmental or biological samples requires all-solid-state sensors with solid contacts for transduction of an ion activity into an electrical signal. Nanostructured carbon materials function as effective solid contacts for this purpose. They can also contribute to improved potential signal stability, reducing the need for frequent sensor calibration. In this Perspective, the structural features of various carbon-based solid contacts described in the literature and their respective abilities to reduce potential drift during long-term, continuous measurements are compared. These carbon materials include nanoporous carbons with various architectures, carbon nanotubes, carbon black, graphene, and graphite-based solid contacts. The effects of accessibility of ionophores, ionic sites, and other components of an ion-selective membrane to the internal or external carbon surfaces are discussed, because this impacts double-layer capacitance and potential drift. The effects of carbon composition on water-layer formation are also considered, which is another contributor to potential drift during long-term measurements. Recommendations regarding the selection of solid contacts and considerations for their characterization and testing in solid-contact ion-selective electrodes are provided.

1. Introduction

Ion-selective sensors are widely used for pH monitoring and ion analysis in health care, environmental analysis, and research applications.[1–3] As an example, blood analyzers with integrated ion-selective electrodes (ISEs) carry out over a billion measurements each year on electrolytes, such as K^+, Na^+, Cl^-, Ca^{2+}, Li^+, Mg^{2+}, and CO_3^{2-}.[4] The conventional ISEs used in these analyzers are reliable but require frequent recalibration and careful maintenance. Because they depend on inner filling solutions to transduce ion activities in the sample to electrical potentials for potentiometric measurements, conventional ISEs are difficult to miniaturize. These limitations can be overcome using all-solid-state ISEs, which enable new applications of ISEs such as in the quickly expanding field of wearable and implantable sensing devices.

In such all-solid-state ISEs, a solid contact replaces the inner filling solution.[5–8] The solid contact material is sandwiched between an electron-conducting substrate (typically gold, glassy carbon, or another carbon conductor) and an ion-selective membrane (ISM) (**Figure 1a**).[9,10] The ISM is composed of a polymer, often in combination with a plasticizer, an ionophore (a hydrophobic molecule that acts as a specific ligand for the target ion and has a very low solubility in the aqueous sample phase), and highly hydrophobic ionic sites to balance charge in the ISM.[11] When target ions are in equilibrium between the sample and the membrane, a potential is established at that interface, following the Nernst equation.[12] Signal transduction, that is, the conversion of an ion activity into an electrical response, then occurs at the solid contact by one of two mechanisms. When conductive polymers are used as the solid contact, the polymers can conduct both ions and electrons, and they exhibit high redox capacitance as they convert the charge carrier from ions to electrons through doping/undoping of the polymer.[9] Unfortunately, conductive polymers can be sensitive to light, oxygen, and carbon dioxide interferences, and they can also suffer from unstable potentials resulting from the possible formation of a water layer between the ISM and the conducting polymer (**Figure 2**).[13–16] These problems may be circumvented by using nanostructured carbon materials with high specific surface areas as solid contacts. Transduction from ion conduction in the ISM to electron conduction using carbon-based solid contacts relies on the formation of an electrical double layer at the interface between the ISM and the carbon surface. The corresponding interfacial potential is a function of the quantity of charge in the double layer. The overall potential is the sum of the potentials at the interface between the electron-conducting substrate and the solid contact (which, as a contact potential between two electron-conducting materials, is a constant given by the bulk properties of the carbon and the solid contact),[17] the interface between the solid contact and the ISM (a potential minimized by high capacitance), and the interface between the ISM and the sample (a phase boundary potential that follows the Nernst equation). Direct contact of the ISM with the electron-conducting substrate through pores and inter-particle voids of the solid-contact material is possible and

Y. E. Chipangura, B. D. Spindler, P. Bühlmann, A. Stein
Department of Chemistry
University of Minnesota
207 Pleasant St. SE, Minneapolis, MN 55454, USA
E-mail: buhlmann@umn.edu; a-stein@umn.edu

The ORCID identification number(s) for the author(s) of this article can be found under https://doi.org/10.1002/adma.202309778

DOI: 10.1002/adma.202309778

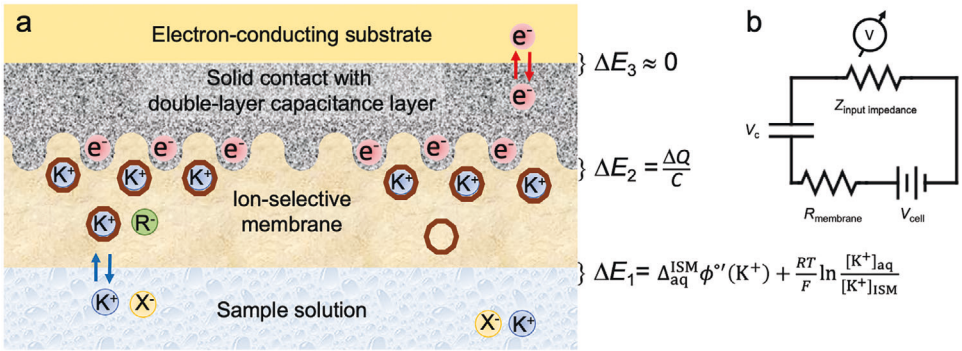

Figure 1. a) Schematic diagram of a solid-contact ion-selective sensor electrode (SC-ISE), showing the four phases involved during sensor operation (electron-conducting substrate, electric-double-layer forming solid contact, ion-selective membrane (ISM), and aqueous sample solution), the species present in each phase, and the corresponding interfacial potentials. The brown circles refer to a K^+-selective ionophore, R^- to anionic sites, X^- to counter anions in solution, K^+ to free potassium ions, and K^+ surrounded by a brown circle to K^+–ionophore complexes. Q = charge, C = capacitance, $\Delta_{aq}^{ISM}\phi^{o\prime}(K^+)$ = standard ion transfer potential of K^+ from the ISM to the aqueous phase.[5] b) Simplified equivalent circuit of an ion-selective sensor with a solid contact. The solid contact is represented by the capacitance C, the largest sensor resistance (that of the polymeric membrane) by $R_{membrane}$, the potential difference between the ISE and the reference electrode by the voltage source, V_{cell}, and the input impedance by $Z_{input\ impedance}$.

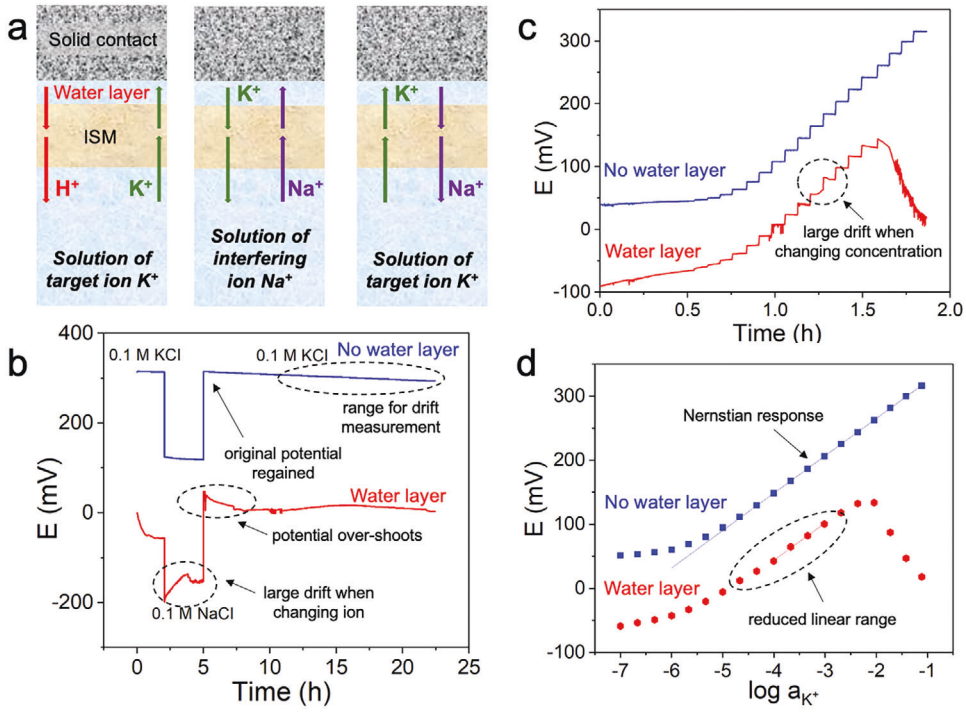

Figure 2. Effects of a water layer between the solid contact and the ISM, illustrated for a K^+-selective ISE and Na^+ as an interfering ion. a) Schematic showing the ion transport at interfaces between the sample, the ISM, a water layer, and the solid contact. The water layer introduces new interfacial potentials that are controlled by the ion concentrations in this layer and depend through transmembrane ion fluxes on the sample composition. b) Response of electrode potentials when the ISE is first exposed to 0.1 M KCl solution, then to 0.1 M NaCl solution, and then again to the 0.1 M KCl solution. In the absence of a water layer, the initial potential should be constant after the electrode is equilibrated. The potential should then drop rapidly when K^+ is replaced by Na^+ and return rapidly to the original potential after exchanging Na^+ with K^+ again. When a water layer is present, drift can be observed at the various stages of this test, and the potential before the switch to the NaCl solution differs from the potential after the change back from NaCl to KCl. c) Especially for thin ISM membranes, drifts in potential after changing the ion concentration in the sample can also be an indication of water layer formation, as seen in these dynamic response curves. d) In the presence of a water layer, the calibration curves may be non-Nernstian and the linear response range may be reduced.

typically not a problem, but the contribution of the ISM/solid-contact material to the total capacity of the device usually by far exceeds the ISM/electron conductor capacity.

Stabilization of the sensor's potential is one requirement toward the goal of achieving calibration-less or calibration-free sensors. Potential drift can arise from multiple sources, for example, from changes in composition of the ISM if membrane components leach out of the membrane, continued curing/cross-linking of the membrane, or the formation of a water layer.[18–20] Another cause of potential drift of a solid-contact ISE with a capacitive interface is related to current flow through the sensor circuit. The potential drift or change in potential with time equals $\Delta E/\Delta t = i/C$, where i is the current and C is capacitance. Ideally, no current should flow in a potentiometric measurement. In reality, the current is nonzero and depends on the input impedance of the voltmeter, the resistance of the ISM, the voltage of the cell, and the capacitance of the solid contact at its interface with the ISM. The latter parameter is controlled by the surface area of the solid contact, which is a function of carbon morphology when nanostructured solid contact materials are used. A higher capacitance results in smaller signal drift. Thus, outstanding stability in potential has been achieved in recent years with sensors using nanostructured carbon as the solid contact.

To estimate the potential drift caused by charging of the capacitive interface of the ISM and the underlying solid contact, the ISE setup can be thought of as a serial combination of R and C, where the solid contact acts as an asymmetric double-layer capacitor, and the resistance is typically limited by the polymeric membrane phase (Figure 1b). The potential difference between the ISE and the reference electrode is the DC voltage measured by a high input impedance voltmeter. When the circuit is closed, a small current will flow, very slowly charging up the capacitor, resulting in signal drift. With the very high input impedance of the voltmeters that are typically used in research (≈10 TΩ), the current is extremely small for most situations, and exceptionally small signal drifts can be achieved. However, for the design of economical, self-contained, wearable sensors, such a high impedance may not be feasible, and a larger current would result in larger potential drifts. This can be counteracted by using a solid contact with a higher double-layer capacitance, given certain criteria that must be fulfilled and that will be discussed later in this Perspective article. The need for solid contacts with high specific capacitance becomes even more important in the case of highly miniaturized sensors, such as microneedle array sensors.

For systems of practical relevance, the input impedance of the voltmeter is much larger than the resistance of the ISE membrane, R_{mem}. Assuming that there is no potential across the capacitive interface, V_C, at the start of the measurement ($t = 0$), and that a current limited by the input resistance, R_{in}, of the voltmeter flows through the cell as soon as the measurement is started (charging up the capacitor until $V_c = V_{cell}$), the potential across the capacitor and the potential measured with the voltmeter, V_m, are given by Equations (1) and (2), respectively.

$$V_c = V_{cell}\left(1 - e^{\frac{-t}{R_{in}C}}\right) \tag{1}$$

$$V_m = V_{cell} - V_c \tag{2}$$

Figure 3 illustrates the predicted time dependence of V_C and V_m for $V_{cell} = 500$ mV, $R_{in} = 10$ TΩ, and three representative capacitances.

The expression for drift of V_m is obtained from the derivative of Equation (2) with respect to time, giving Equation (3).

$$\frac{dV_m}{dt} = -\frac{V_{cell}}{R_{in}C}e^{\frac{-t}{R_{in}C}} \tag{3}$$

As illustrated by Figure 3c for different values of C, the largest drift occurs immediately after the start of the measurement but eventually decreases with time. The x–axes of Figures 3a–c are shown in years to highlight the expected charging of the capacitive interface. However, drift on the time scale of days or weeks is usually of interest, and longer term drift may also be affected by other factors. Moreover, the thus predicted drift is largest at the start of the experiment. This value can be obtained by evaluating Equation (3) at $t = 0$, giving Equation (4), which is most relevant for designing sensors for applications in continuous monitoring.

$$\left.\frac{dV_m}{dt}\right|_{t=0} = -\frac{V_{cell}}{R_{in}C} \tag{4}$$

The minimum frequency of sensor recalibration depends on sensor drift and the acceptable error for a given application. If it is impractical to recalibrate a sensor during operation (such as, for a wearable or implantable sensor), then one can determine the maximum allowable drift to keep the measurement error under the acceptable limit for the duration of use. For a pre-defined maximum allowable drift and assuming that charging of the carbon/membrane interfacial capacitance is the only factor determining potential drift, one can obtain the minimum capacitance required at the membrane/carbon interface for an SC-ISE paired with a voltmeter with a given R_{in} by inserting the respective values into Equation (4). The specific capacitance of the solid contact material is also of high importance; the minimum mass (m) of carbon required to achieve a pre-defined drift decreases with increasing specific capacitance, C_s (Equation (5)).

$$m = \left|\frac{V_{cell}}{R_{in}C_s\left.\frac{dV_m}{dt}\right|_{t=0}}\right| \tag{5}$$

The input impedance, double layer capacitance, and mass of carbon required to target a maximum drift of the measured potential are all important factors to consider when designing SC-ISEs for a specific application. The combination of these factors becomes especially important when designing SC-ISEs with small form factors because the amount of solid contact material that can fit onto a small electrode is limited. Figure 3d shows the effect of specific capacitance and input impedance on the minimum mass of carbon required to achieve an initial drift of 1 μV h^{-1} for a cell with $V_{cell} = 500$ mV. Two types of porous carbon are chosen for illustration, colloid-imprinted mesoporous (CIM) carbon and three-dimensionally ordered macroporous (3DOM) carbon, see Section 2. For a voltmeter with an input impedance of 10 TΩ, a minimum of 9 μg CIM carbon ($C_s = 20$ F g^{-1}), 100 μg 3DOM carbon ($C_s = 1.8$ F g^{-1}), or 1800 μg of carbon with $C_s = 0.1$

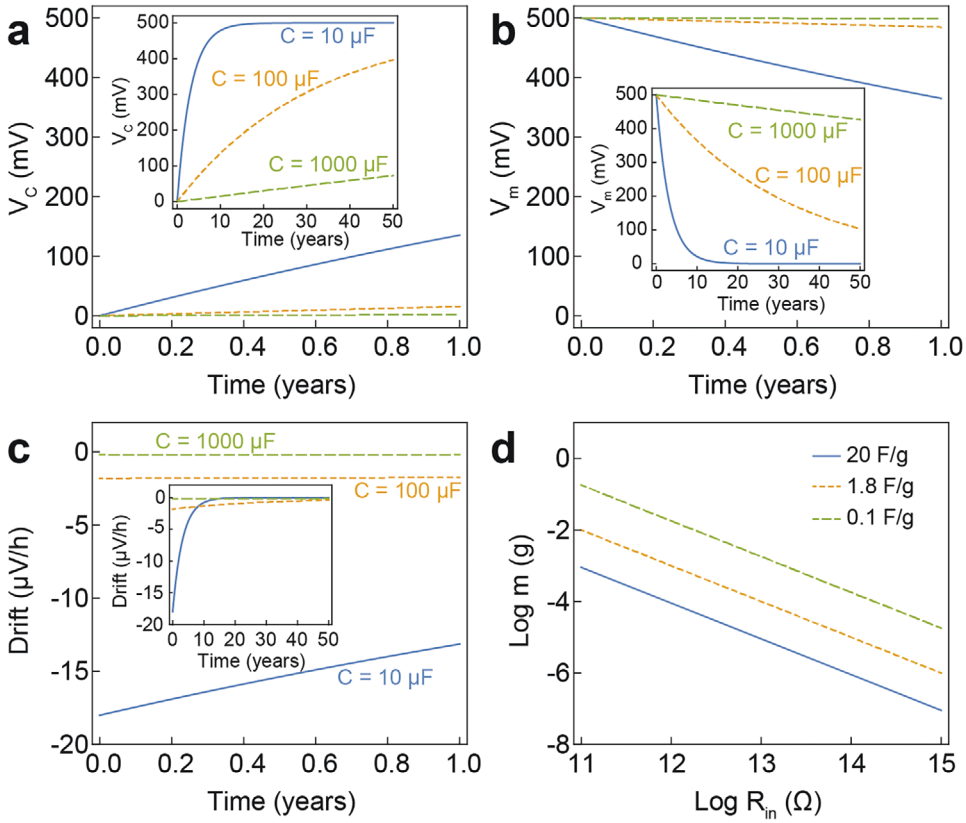

Figure 3. Theoretically predicted drift of SC-ISEs when caused exclusively by charging of the electric double layer at the carbon/ISM interface. a) Potential across the capacitor, V_C. b) Measured potential, V_m, across the voltmeter after the circuit is closed (assuming V_{cell} = 500 mV, $R_{in} + R_m$ = 10 TΩ). c) Drift of V_m after the circuit is closed with V_{cell} = 500 mV and R_{in} = 10 TΩ. d) Influence of specific capacitance and input impedance on the minimum mass of solid contact material required to achieve a drift of 1 μV h^{-1} for a cell with V_{cell} = 500 mV. C_s values of 20 and 1.8 F g^{-1} are values reported for CIM and 3DOM carbon, respectively. The value of 0.1 F g^{-1} was included for illustration purposes only.

F g^{-1} is required to achieve a drift of 1 μV h^{-1}. Therefore, choosing a solid contact material that has a high, accessible surface area is critical for use in sensors with small form factors.

The values of 20 and 1.8 F g^{-1} for CIM and 3DOM carbon, respectively, were obtained from measurements in solutions of acetonitrile with an electrolyte comprised of ions of smaller size ($TEA^+BF_4^-$) than the ionophore–ion complexes and bulky counter-ions present in an ISM. However, values of specific capacitance obtained in simple electrolyte solutions may be much higher than specific capacitances for SC-ISEs in contact with an ISM, in particular if the carbon used contains a large number of micropores. Thus, when considering carbon materials for application in SC-ISEs, it is important to measure specific capacitance of the carbon in the actual SC-ISE, and not just the capacitance of the carbon material in a solution of an arbitrary electrolyte.

2. Carbon Materials as Solid Contacts

While various forms of carbon have been investigated as solid contacts for ISEs, all contain graphitic domains or graphene-derived units mainly composed of sp^2-hybridized carbon, allowing electron delocalization and electrical conduction. In the case of supercapacitors, it may be desirable to enhance conductivity for high power applications, for example by doping the carbon with nitrogen. For ISEs used in potentiometric measurements, such conductivity enhancements are not required for ion-to-electron transduction, as ideally, no current should flow during the measurement, and in practice, any current is extremely small. In fact, dopant sites and oxygen groups should be avoided, as these can become redox-active and can result in less controllable potentials. Such groups can also make the carbon more hydrophilic, thus contributing to problems associated with the formation of a water layer at the carbon/membrane or carbon/current collector interfaces.[21,22] Furthermore, functional groups at carbon surfaces that can be protonated or deprotonated render the phase boundary potential at these surfaces sensitive to the pH.

In terms of morphology, the simplest carbon contact is a glassy carbon electrode with a planar surface. However, in terms of ion-to-electron transduction, such a flat surface is not very effective, given that the surface area and thus the electric double layer capacitance are small. Exposed areas of typical glassy carbon electrodes used for solid-contact ISE fabrication fall in the range from 0.02 to 0.07 cm^2. In contrast, an electrode coated with 1 mg of nanostructured carbon having a specific surface area of 400 m^2 g^{-1} has an interfacial area that is about five orders of magnitude larger. Assuming that all of this surface is accessible to the ionophore–ion complexes and anionic sites, this would translate

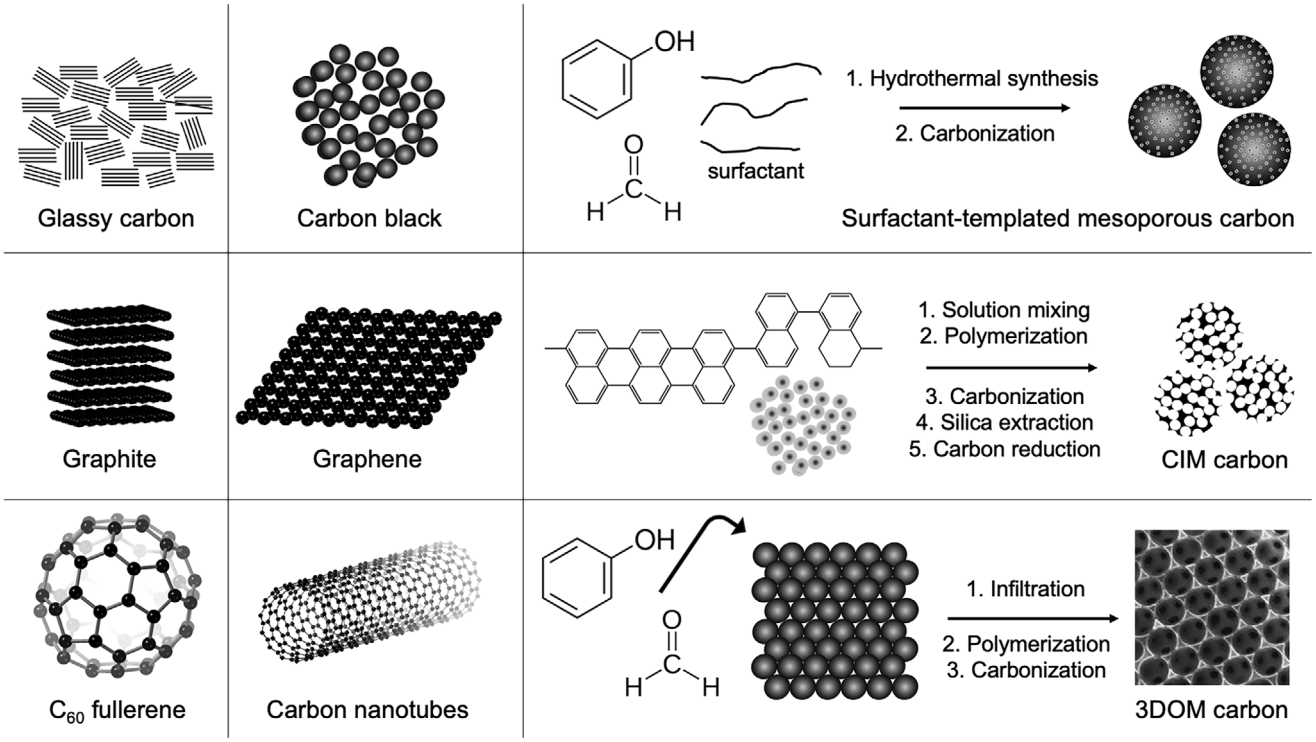

Figure 4. A selection of carbon materials used as solid contacts in ion-selective electrodes. The schemes of graphite, graphene, C_{60}, and carbon nanotubes were made using CrystalMaker X from CrystalMaker Software. For the templated nanoporous solid contacts, the templating processes are also shown.

into a much higher double layer capacitance and, as a consequence, a smaller drift in measured potential if any current flows through the sensor circuit. In this section, we discuss the major types of carbon that have been used as solid contacts in ISEs (see **Figure 4**) and their features that are relevant to ISE performance.

2.1. Graphite

Early studies of carbon-based solid-contacts in ISEs employed graphite as the ion-to-electron transducer. From a crystallographic standpoint, an ideal graphite crystal, a 2D material consisting of many layers of parallel graphene sheets would be nonporous with a theoretical density of 2.26 g cm^{-3} However, this density is observed only in highly ordered pyrolytic graphite (HOPG).[23] As a result of the weak van der Waals interactions between the sheets and kinetic trapping of structural irregularities during the formation processes of most natural and artificial graphite, unavoidable defects in real graphite materials can introduce internal porosity that is not well defined. Synthetic graphite is often made by mixing a petroleum-coke flour with a coal-tar pitch binder, extruding the mixture, baking it at about 1000 °C, and then graphitizing it between 2500 and 3000 °C.[24] The density of the resulting graphite can be as low as 1.6 to 1.7 g cm^{-3}, implying up to 30% porosity, with non-uniform pores throughout the material. Through tomographic analysis, a wide range of pore types with sizes between 70 nm and 5 µm was revealed in graphite electrodes,[25] but surface areas in graphite powders tend to be relatively small (one review lists a range of 9–24 m^2 g^{-1}).[26]

Ruzicka and co-workers took advantage of this porosity over 50 years ago, when they developed so-called universal ISEs ("Selectrodes"), in which graphite rods were impregnated with a liquid organic phase containing an ionophore.[27–29] At that time, the authors already claimed that the electrodes showed no drift over 5 weeks. This work was followed nearly three decades later by Chaniotakis and co-workers, who used a highly conductive porous carbon rod (compressed charcoal) as the solid contact, which was infiltrated with an organic phase, such as ionophore-doped plasticized poly(vinyl chloride) (PVC).[30,31] As an interesting side-note, Chaniotakis already suggested the application of this approach in microsensor arrays, which to that point had been prepared with aqueous inner filling solutions or solid contacts such as metallic silver and silver epoxy. Graphite rods impregnated with an ionophore have also been used as solid contacts in ISEs for high pressure measurements.[32] When considering graphite and related materials as solid contact, the carbon purity is critical. While basal planes of graphite are relatively inert, edges are more reactive and can become the sites of acidic surface oxides, rendering the surface hydrophilic and pH sensitive.[29] In contrast, graphite free from chemisorbed oxygen is hydrophobic. Another related material that has been used for the preparation of solid contact ISEs is the so-called nanographite,[33,34] which consists of irregularly sized platelets of varying thickness. The dimensions of these platelets depend strongly on the method of fabrication from graphite, and while nanographite materials with submicrometer dimensions have been reported, commercial products that were used for ISE fabrication had particle size distributions in the range of 0.10 to 10 µm.

Brunauer–Emmett–Teller (BET) analysis shows a broad distribution of micropores and mesopores in nanographite particles and surface areas on the order of 150 m^2 g^{-1},[35] depending on the method of fabrication.

Recently, graphite-based carbon paste was screen-printed onto a polyethylene terephthalate substrate[36] and used as both the solid contact and the electron-conducting layer in nitrate ISEs without the need for an additional metallic charge collector.[37] The authors claimed that in this case, introduction of oxygen-containing functional groups (hydroxyl, carboxyl, carbonyl) on the printed carbon surface by cold atmospheric plasma treatment was beneficial for introducing covalent bonds between the carbon electrode and PVC-based the ISM. In this configuration, removal of surface contamination on the carbon by the plasma treatment helped to reduce water layer formation. In addition, due to the double-function of the graphite layer, any void space between a solid contact and another electron conductor was eliminated, also making water layer formation less likely.

2.2. Glassy Carbon

Another type of carbon that is frequently used as an electrode in electrochemical applications is glassy carbon, also called vitreous carbon. In this material, small domains of multiple graphene layers and other graphene-like units are randomly oriented and do not form an extended graphite structure even at high temperature (a "non-graphitizing" carbon) except under specific high-stress conditions.[38] This enhances the hardness of the carbon compared to graphite, while maintaining sufficient electrical conductivity for use in electrodes. Fouskaki et al. used a high purity, porous glassy carbon prepared from a synthetic phenolic resin precursor as both the support for the liquid polymeric membrane and as solid contact.[39] They infiltrated the randomly structured pores with a cocktail containing the ionophore, plasticizer, and ionic additive and placed a thin PVC membrane at the front of a glassy carbon monolith. Although an excellent lower detection limit was reported for Pb^{2+}-ISEs made with these sensors, calibration curves showed significant potential drift.

2.3. 3DOM Carbon

Among carbon solid contacts with more designed structures, the first materials reported were 3DOM carbon monoliths with highly interconnected, uniform macropores (**Figure 5**a).[21,22,40–43] All-solid-state ISEs with 3DOM carbon solid contacts exhibited the required Nernstian response and provided several advantages over earlier developed ISEs with conductive polymers as the solid contact. These advantages included less drift in the potential over time, which would necessitate fewer calibrations (potential drift: 12 μV h^{-1} over 70 h), less sensitivity to oxygen or carbon dioxide interferences, and a reduced tendency for water layer formation (which would contribute to drift). 3DOM carbon is prepared by infiltrating a fluid carbon precursor into a polymeric colloidal crystal template, polymerizing the precursor throughout the template, and then carbonizing it.[22,44–47] As the template is removed during thermal processing, a pore structure is produced that replicates the geometry of the original template. With a template consisting of uniform spheres, close packed in a face-centered cubic pattern, a bicontinuous structure is obtained, consisting of an electrically conducting carbon phase (e.g., 0.34 S cm^{-1})[22] and a continuous pore space with spheroidal macropores that are interconnected in three dimensions through circular windows at those points where the original template spheres touched each other. This structure has a highly textured surface, contains a relatively large internal surface area, and can be fully penetrated by the ISM, including the membrane polymer, plasticizer, ionophore, and ionic sites (Figure 5b).[21] The pore texture can make the surface of 3DOM carbon particles superhydrophobic through Wenzel or Cassie effects,[48] which helps to exclude a detrimental water layer. As an alternative method, interference lithography has been used to prepare similar structures.[49]

A variety of precursors can be employed to form 3DOM carbon, resulting in macropore walls composed of glassy carbon, graphite, or even diamond.[44,45] In the context of ISEs, so far only resol-based precursors (phenol–formaldehyde, resorcinol–formaldehyde) have been employed for 3DOM C solid contacts, or in the case of lithography, a negative resist was used as a precursor. The resol precursors form a glassy carbon structure that also includes some oxygen in the form of ketone or phenolic groups. Depending on synthesis details, BET surface areas in the range from 140 to 340 m^2 g^{-1} have been reported for 3DOM carbon with a size of the templated pores of ≈300 nm, but about 2/3 of that area is due to micropores with diameters less than 2 nm (the theoretical specific surface area of 300-nm close-packed voids in a glassy carbon matrix with smooth walls would be ≈36 m^2 g^{-1}). Through treatment with oxidizing acids, additional lactone, lactol, and carboxylic acid groups can be introduced, a process that further increases the pore volume and BET surface area of the carbon and also raises its capacitance significantly. However, for use in solid-contact ISEs, this procedure is not desirable. Instead, the oxygen content should be minimized to avoid spurious redox-active groups and to maintain high hydrophobicity to prevent water layer formation.[21] This can be achieved by increasing the carbonization temperature (900 °C was used in ISE studies). Much higher pyrolysis temperatures can be used to increase the degree of graphitization. Additional reduction of the porous carbon in a hydrogen atmosphere can further reduce the oxygen content. Besides redox-active groups, edge defects in the carbon structure may decrease the potential stability, as observed for lithographically prepared pyrolyzed carbon with 3DOM structure, which was converted to a more graphenic phase by coating with nickel, thermal annealing, and removal of nickel by etching.[49] (Residual nickel may also have contributed to the decrease in stability.)

It is notable that even with its large pore size and associated windows between pores close to 100 nm in diameter, some segregation of plasticizer and PVC was noted for 3DOM carbon solid contacts: the PVC content of the ISM material in the macropores was approximately one third lower than that in the bulk ISM.[21] This is likely due to the smaller diffusion coefficient of the polymer as compared to the plasticizer, although different surface interactions between ISM components and the carbon walls should also be considered as possible contributing factors. Viscosity also limits the extent of macropore infiltration: filling fractions ranged from 25% with 66 wt% plasticizer to 9% with 33 wt% plasticizer. While ISEs with these different

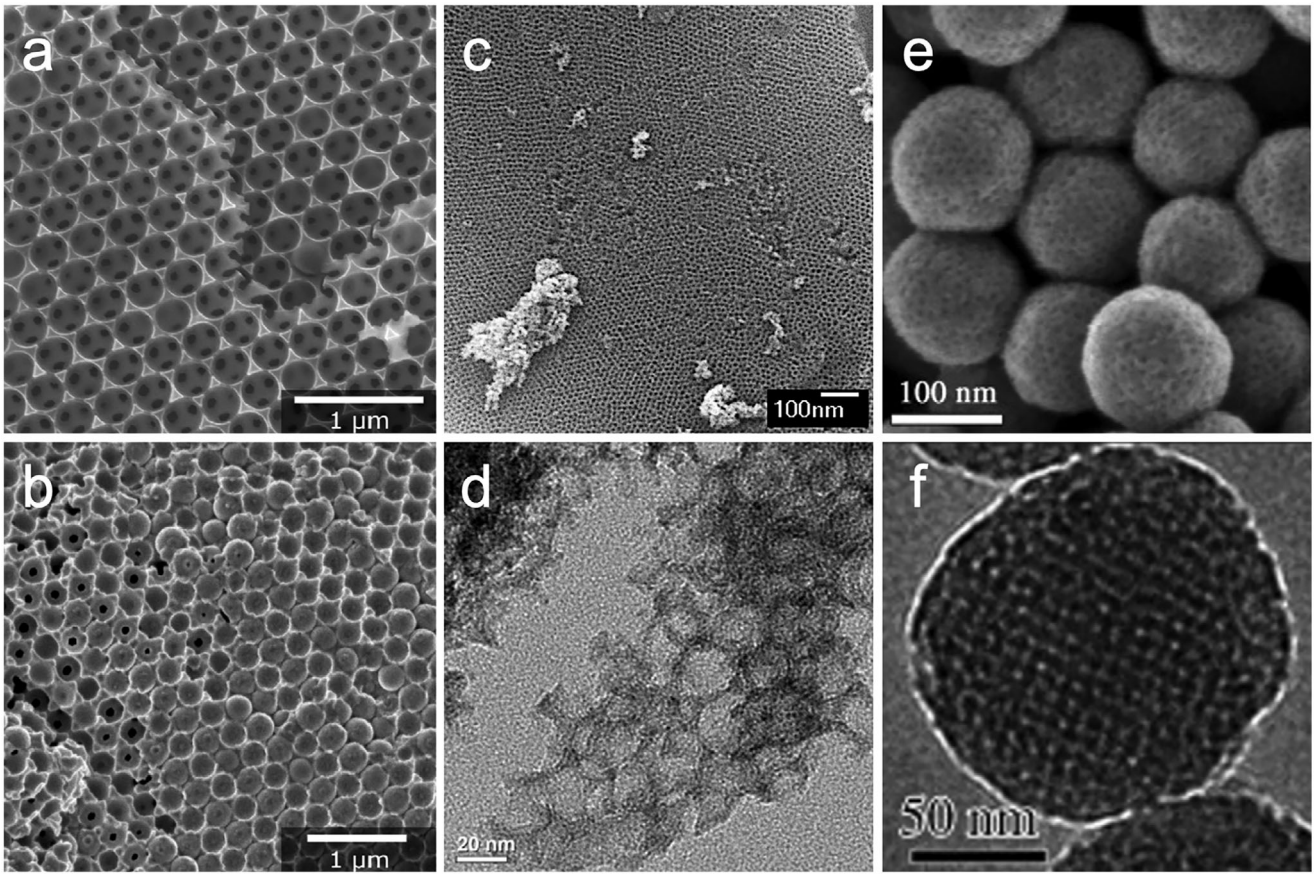

Figure 5. Electron microscopy images of various porous, nanostructured carbon materials used as solid contacts for ISEs. a) SEM image of 3DOM carbon. b) SEM image of 3DOM carbon infiltrated with sensing membrane materials consisting of PVC, plasticizer, ionophore, and ionic sites. Reprinted with permission.[21] Copyright 2010, American Chemical Society. c) SEM image of CIM carbon. Reprinted with permission.[52] Copyright 2023, American Chemical Society. d) TEM image of CIM carbon. Reprinted with permission.[53] Copyright 2014, American Chemical Society. e) High-resolution SEM and f) TEM images of ordered mesoporous carbon spheres. Reprinted with permission.[54] Copyright 2010, Wiley-VCH.

polymer:plasticizer ratios exhibited Nernstian responses, in the case of 3DOM carbon based Ag-ISEs, detection limits could be lowered by increasing the PVC:plasticizer ratio,[40] which lowers ion fluxes.[50,51]

2.4. CIM Carbon

The pore sizes in 3DOM carbon solid contacts investigated so far have been about 300 nm or higher.[22,49] Because the specific surface area of porous carbon materials scales inversely with pore size, one can expect an increase in achievable capacitance and drift stability by decreasing the pore size. The next iteration among carbon solid contacts with designed porosity, therefore, involved templating with smaller colloids to produce three-dimensionally ordered mesoporous (3DOm) carbon with periodic pore structure[55] or CIM carbon with uniformly sized, but less periodic spheroidal pores (Figure 5c,d).[53,56–60] CIM carbon was first described by Jaroniec et al.,[61–63] who used it for sorption and chromatography applications.[64,65] It was later also employed as an electrocatalyst support in proton exchange membrane fuel cells or for formic acid oxidation.[66–68] Stein and Bühlmann introduced CIM carbon as a highly effective solid contact for ISEs[53] and reference electrodes[56,69] and demonstrated record potential stability for K^+-ISEs with this solid contact at that time. CIM carbon can be applied to the electron-conducting substrate by coating the substrate with a carbon–binder dispersion through dropcasting[53,56,70] or by attaching a preformed, roller-pressed carbon–binder film to the substrate.[52] For the synthesis of CIM carbon, colloidal silica is the template of choice, because it can be produced more monodisperse in the size range below 100 nm than polymer spheres. In fact, commercial colloidal silica that is produced on a large scale (e.g., Ludox silica) is suitable for the preparation of CIM carbon. For example, Ludox AS-40 was used for CIM carbon solid contacts reported so far and produces ≈24–26 nm mesopores. Other colloidal silica templates are available in various sizes to achieve mesopore sizes between about 10 and 50 nm. For an ideal colloid-templated carbon structure with close-packed spherical pores, the theoretical specific surface area can be increased from 36 $m^2\ g^{-1}$ for 300 nm pores, to 430 $m^2\ g^{-1}$ for 25 nm pores, and to 1075 $m^2\ g^{-1}$ for 10 nm pores. Actual specific surface areas may be higher due to additional microporosity introduced during the carbonization process. If pores are reduced to even smaller sizes, one needs to take into

consideration accessibility of the ionophore, ionic sites, and matrix into the pores. Small mesopores and micropores may exclude the ionophore and hydrophobic ionic sites through size or transport effects, thus reducing achievable capacitance in the electrical double layer. In addition, one must consider the possibility of mesopores sequestering components of the membrane during preparation as a result of capillary forces or strong physical or chemical interactions between the carbon surface and the component. For example, in the fabrication of silicone-based reference electrode membranes supported on CIM carbon solid contacts, rapid depletion of the ionic liquid from the reference membranes was observed.[52] This was explained by quick penetration of the solution of membrane precursors into the CIM carbon pores, followed by replacement of solvent molecules in the pores with ionic liquid from the overlying reference membrane, driven by evaporation of the solvent from the surface of the reference membrane into the ambient air. The silicone precursors in the curing reference membrane quickly polymerized to an extent that they could no longer penetrate the CIM carbon pores. As a result of the depletion of ionic liquid in that membrane, the membrane resistance increased to the point that the device no longer functioned. To avoid this problem, either an excess of ionic liquid needs to be added to the membrane solution or the mesopores can be presaturated with ionic liquid before adding the remaining membrane solution. Similar sequestration by a high-surface area carbon can occur in the case of ionophores that interact strongly with the carbon surface, as observed for the K^+ ionophore BME-44 and CIM carbon.[52]

A second advantage of CIM carbon over resol-derived 3DOM carbon concerns the carbon precursor. For CIM carbon, a mesophase pitch is used, which is a highly polyaromatic material with very low oxygen content. In the preparation of CIM carbon, some oxygen (4–6 wt%) is introduced during removal of the silica template by etching with potassium or sodium hydroxide, introducing ketone, phenol, and carboxylic acid groups that make the material hydrophilic.[71] While functionalization of the CIM carbon with fluorinated groups is one approach to form a hydrophobic material,[72] in the context of solid contacts for sensor electrodes, a simpler approach is treatment at high temperature (1500 °C) in an inert gas (N_2)[71] or at slightly lower temperature (900 °C) in a reducing gas (5% H_2, 95% N_2) to remove most oxygen atoms from the carbon surface (remainder: 0.2–0.4 wt%).[53] ISEs using CIM carbon treated by the latter approach did not form any water layers during sensing in aqueous solutions, and they exhibited a very small drift of 1.3 μV h^{-1} over 70 h for a potassium-ISE.[53] In contrast to the 3DOM carbon monoliths, CIM carbon powders are suitable to form inks that can be used to coat gold or glassy carbon electrodes, as well as paper[56,57] or polymer (PET) substrates[58] to form ISEs or reference electrodes.

2.5. Other Mesoporous Carbon Materials

Other porous carbon solid contacts that have been investigated include ordered mesoporous carbon (3.8–4 nm pores, long-term drift not reported but short term drift 28 μV s^{-1} at 1 nA compared to 1 μV s^{-1} at 1 nA for CIM carbon and 1.6 μV s^{-1} at 1 nA for 3DOM carbon), disordered mesoporous carbon (50 nm pores, short term drift 29 μV s^{-1} at 1 nA), mesoporous carbon nanospheres templated using block-copolymer surfactants (Figure 5e,f; ≈2.35–3 nm pores; 28 μV h^{-1} over 70 h), and microporous carbon spheres (<2 nm pores; 14.9 μV h^{-1} over 20 h).[73–75] Multiple potential causes may be responsible for the poorer performance of these materials. The ordered and disordered mesoporous carbons were obtained from a commercial source, and the corresponding precursors and processing conditions were not provided.[73] However, cyclic voltammograms of the corresponding electrodes in 0.1 M KNO_3 solution indicated the presence of redox-active groups in these materials. The microporous carbon spheres had a very large surface area of over 2000 m^2 g^{-1}, but all the surface was due to micropores, which may provide only limited access to the K^+ complex of the valinomycin ionophore.[75] Furthermore, these carbon spheres were prepared from dopamine as the precursor and treated with KOH to introduce micropores. This resulted in a high capacitance, but from the reported cyclovoltammogram it is apparent that a large fraction of the capacitance was redox capacitance arising from heteroatom groups. In the case of the mesoporous carbon nanospheres, the largest capacitance and close-to-Nernstian responses were obtained with spheres pyrolyzed at 750 °C, at which point the oxygen content is still very high.[74] This is likely the key factor explaining the potential drifts after stepwise increases in the K^+ activity, as apparent in the reported potential versus time curves; such drifts often indicate the presence of a water layer. **Figure 6** illustrates the various shapes of cyclovoltammograms obtained with carbon solid contacts without or with redox-active groups present.

Whereas access to a high surface area may be limited in some solids with very small pores, most of the surface should be accessible to ion–ionophore complexes, hydrophobic ionic sites, and other ISM components in the case of nonporous, nanostructured, high-surface area carbon materials. These include single-walled carbon nanotubes (SWCNTs),[77–80] multi-walled carbon nanotubes (MWCNTs),[81–90] nanohorns (bud-like structures derived from SWCNTs),[91] buckyballs,[92–94] and certain types of carbon black.[95–97] Certain MWCNTs with thin walls can also contain internal porosity, although infiltration of ionophore molecules may be diffusion-limited in relatively long (micrometer length) but narrow (e.g., 40 nm) channels.[98]

2.6. Carbon Nanotubes

Carbon nanotubes exhibit several features that are desirable for solid contacts. Unless they are specifically functionalized with polar functional groups, they are very hydrophobic and not susceptible to redox reactions at the interfaces to the ISM and at the supporting electronic contact. This helps avoid water layer formation and spurious side reactions. Like the other forms of carbon investigated as solid contacts, carbon nanotubes are not sensitive to light.[78] However, certain types of SWCNTs (zigzag SWCNTs) have small bandgaps[99] and absorb in the near IR region,[100] so that a temperature-dependent response may be expected. Although CNTs can form bundles, they tend to form a relatively open, well-interconnected network structure that should be easily penetrated by ISM components (**Figure 7**a,b). Depending on their conformation, carbon nanotubes are either metallic or semiconducting along the tubular axis. The relatively high

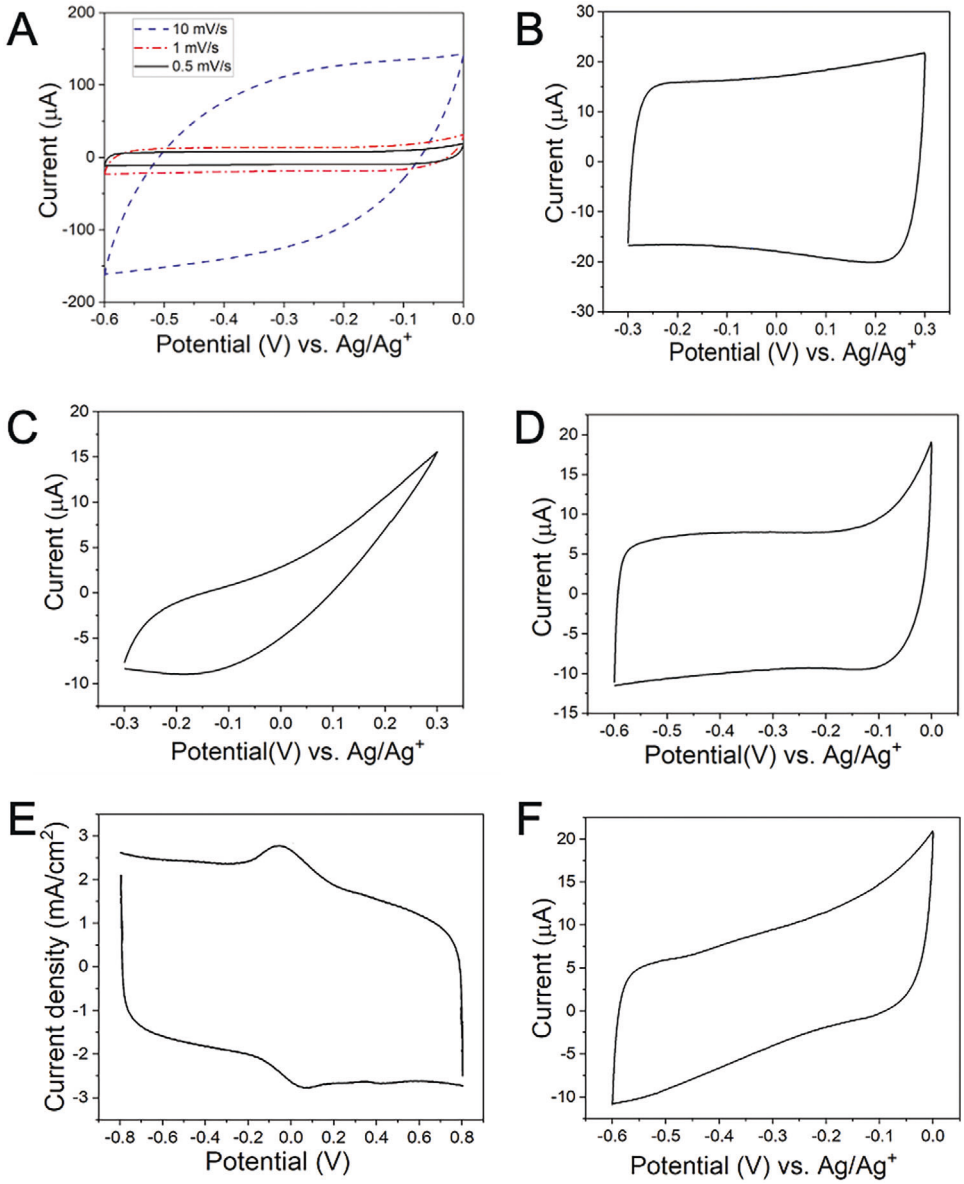

Figure 6. Determination of capacitance with cyclic voltammetry. A) For a voltage-independent capacitance, the ideal CV at low scan rates shows a rectangular shape with voltage-independent currents in both the forward and backward scans. $C = |i_c - i_a|/(2\nu)$, where ν is the scan rate and $|i_c - i_a|$ is the difference between the currents in the forward and backward scan. Too high a scan rate results in characteristic curvatures of the i versus V curve following each change of scan direction. B) Simultaneous increases or decreases of $|i_c|$ and $|i_a|$ as the potential changes are indicative of a voltage-dependent capacitance. C) Large currents, seen here at positive potentials, result from redox reactions of dissolved species, such as solvent, electrolyte, or oxygen. D) Same electrode as for Panel C, but with a shift to a potential window in which there is much less redox activity, restoring the rectangular shape of the CV. E) Current peaks indicative of redox reactions of surface-confined species. Adapted with permission.[76] Copyright 2012, American Chemical Society. F) Relatively high cell resistance, R_{cell}, resulting in ohmic voltage drop ($V_{ohmic} = i\ R_{cell}$) and, therefore, a rhomboid shape of the otherwise mostly capacitive CV.

surface–volume ratios of carbon nanotubes result in large double-layer capacitance. However, surface areas of carbon nanotubes can vary widely. Whereas the theoretical specific surface area for isolated, closed SWCNTs is 1315 $m^2\ g^{-1}$, it is lower in bundles (600 $m^2\ g^{-1}$) and more typically ≈400 $m^2\ g^{-1}$.[101] In the case of MWCNTs, the surface area depends on the diameter of the CNTs, but is typically a few hundred $m^2\ g^{-1}$.

The first report of SWCNTs as solid contacts for ISEs was by Crespo, Macho, and Rius.[77] Spray coating the SWCNTs onto a non-conducting PVC substrate resulted in a ≈25 μm thick film that was electrically contacted with a metal clamp. A potassium-ISE incorporating this solid contact exhibited Nernstian behavior with a dynamic range over four orders of concentration, good selectivity and detection limits, and response times <10 s. Electrochemical impedance spectroscopy (EIS) spectra of SWCNT

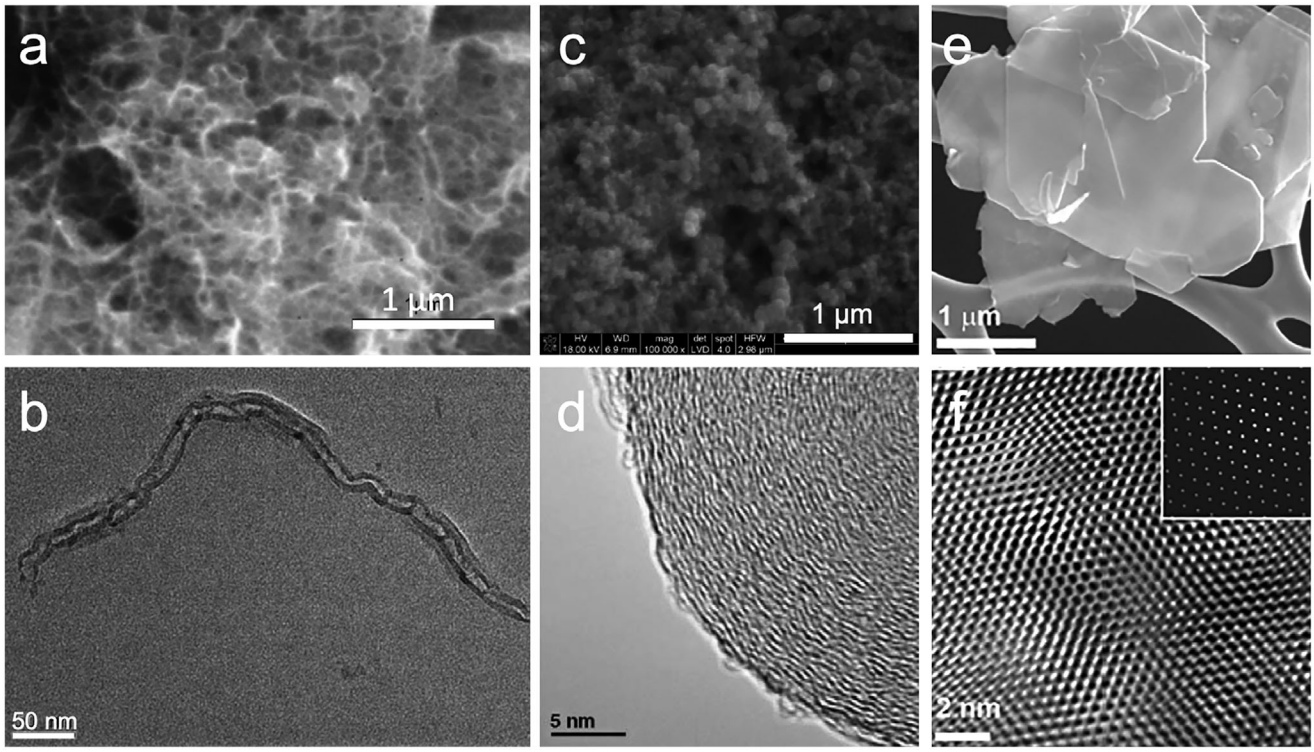

Figure 7. Electron microscopy images of mainly nonporous carbon solid contact materials. a) Environmental SEM image of a carbon nanotube transducer layer. Reprinted with permission.[77] Copyright 2008, American Chemical Society. b) TEM image of a PVC-DOS thin film (100 nm thick) containing 0.5 wt% MWNCTs with 5 wt% surfactant F127. Reprinted with permission.[102] Copyright 2010, Elsevier. c) SEM image of a Vulcan XC-72 carbon black layer. Reprinted with permission.[95] Copyright 2013, American Chemical Society. d) TEM image of non-graphitized carbon black. Reprinted with permission.[26] Copyright 2006, Elsevier. e) SEM image of exfoliated graphene sheets. f) High-resolution TEM image of an exfoliated graphene sheet. The inset is the Fourier-filtered high-resolution TEM image. Reprinted with permission.[103] Copyright 2020, Elsevier.

layers on glassy carbon disk electrodes in contact with an aqueous electrolyte solution showed a large electronic capacitance (≈0.5–5 mF, depending on film thickness and electrolyte), and large diffusional pseudocapacitance related to ion diffusion in electrolyte-filled pores in the SWCNT layer (≈2–4 mF).[78] Detailed characterization of the transduction mechanism in all-solid-state ISEs with PVC membranes and functionalized MWCNTs by synchrotron radiation X-ray photoelectron spectroscopy combined with vibrational spectroscopy confirmed that ion-to-electron transduction is purely capacitive at the ISM/carbon solid contact/metallic conductor interfaces, and no ion transfer was observed.[82] Increasing the number of deposited CNT solid contact layers results in linearly increased capacitance.[104] Increasing the thickness of the CNT film also helps to avoid undesired aqueous layer formation between the ISM and the underlying metal-contact, which can improve response parameters of the electrode (reduced response time for ion detection, reduced potential drift, improved electrode-to-electrode reproducibility, wider linear response range).[86] This may be explained at least partially by the mechanical resistance of the carbon nanotubes to be pushed away from the underlying electron conductor by an emerging water layer. Carbon nanotube inks also permit the construction of flexible sensors, for example, using filter paper,[105] rubber,[80] or cotton yarns as substrates.[106] More recently, functionalized MWCNTs have been incorporated as solid contacts in microneedle-based K^+-ISEs and reference electrodes.[86,107,108]

While carbon nanotube inks are relatively convenient to use as solid contacts in the fabrication of ISEs, both short-term and longer-term potential drifts observed for CNT-based solid contact electrodes for various ions have exceeded those of meso- and macroporous templated carbon materials. Although the cause of this has not been systematically investigated, a comparison of theoretical specific surface areas of spherical voids in a solid (CIM carbon), solid spheres (carbon black), and solid cylinders (CNTs) with identical diameters follows the order spherical voids > solid spheres > cylinders. For diameters of 50 nm, for example, the specific surface areas would be 215, 80, and 53 $m^2\ g^{-1}$, respectively. This would then translate to the order of the double-layer capacitance, so that on this criterion alone, one would expect nanotubes to have the highest drift value. In line with this argument is the observation that carbon black particles with 50 nm diameter have reported long-term drifts between 10 and 18 $\mu V\ h^{-1}$ for NO_3^- and K^+ measurements, respectively, in between those observed for CIM carbon and CNTs. A limitation of CNTs could be the presence of impurities, such as the metal catalysts incorporated in CNTs during their synthesis or functional groups at open ends of the tubes.[109] Notably, CNTs are known to readily form bundles, which are difficult to disperse and might be expected to reduce a device's capacitance. However, the specific capacitance of SWCNT-coated gold electrodes in NPOE solutions of a range of electrolytes was found to be of 25 to 41 F per gram of carbon.[110] This rather high value suggests that CNT

aggregation does not have to be a major limitation of CNT solid contacts.

2.7. C_{60} Fullerenes

Buckyballs (C_{60} fullerene structures) have also been considered in the context of ISEs. Pure fullerenes are not electrically conductive but become conductive after doping with alkali metals.[111] They are redox-active and act as effective acceptors for multiple electrons that can in turn be oxidized electrochemically.[94] C_{60} molecules covalently attached to a gold substrate were first used in ISEs at the turn of the century, when they were intended as redox-active solid contacts. Drifts observed with these ISEs were relatively small when polymer matrixes were used that did not cause formation of a water layer, but as with much of the work in those days, long-term drifts were not quantified under the well-controlled experimental conditions expected of high-quality work at the present time (see Section 4).[92,93] Later, a K^+-selective electrode with a C_{60} solid-contact[94] and porous C_{60} microcrystals in Pb^{2+}-ISEs were reported.[112] However, the capacitance values of these solid contacts were comparatively low, and potential stability was unremarkable, mainly because the C_{60} molecules are highly aggregated in the microcrystals that were used, so that the effective specific surface areas were significantly lower than one would expect for isolated buckyballs. Even in the case of C_{60} microcrystals with observable macropores, the nitrogen sorption isotherms were of type III,[113] typical for macroporous materials with no identifiable monolayer formation of the adsorbate; they did not show the rise at low relative pressure associated with micropores or the step at intermediate pressures typical for mesoporous materials, so that the effective surface area remained small.[114]

2.8. Carbon Black

Carbon black, a carbon material produced industrially on a large scale as a pigment, reinforcing phase, and conducting additive, is made by decomposing liquid or gaseous hydrocarbons at elevated temperature under a reduced pressure of oxygen. Primary particles consisting of several graphene-like layers combine to form aggregates of various shapes in the size range between 5 and several 100 nm (Figure 7c,d).[26] For example, Vulcan XC-72 carbon black consists of particles with an average size of 50 nm. Aggregation of these particles creates textural mesopores with an average diameter of 19 nm between the particles (BET area: 232 $m^2\ g^{-1}$)[115] that are readily penetrated by the ISM components. Among carbon materials without designed porosity, carbon black-based solid contacts have resulted in the lowest potential drifts observed so far (9.7 $\mu V\ h^{-1}$ over 172 h for a NO_3^- sensor),[95,97] possibly because they can pack more densely than carbon nanotubes while still maintaining pores between particles. Decorating the carbon black with Pt nanoparticles enhanced the electrochemical surface area even further and reduced the long-term drift to 8.2 $\mu V\ h^{-1}$ for a K^+ sensor and to 6.3 $\mu V\ h^{-1}$ for a NO_3^- sensor over a 172 h period.[95] The drift was slightly higher for a K^+-sensor relying on a different type of carbon black (Printex XE-2, 9–15 $\mu V\ h^{-1}$ over 72 h), even though the average primary particle size is smaller for Printex XE-2 (30 nm), and its BET surface area significantly higher (910 $m^2\ g^{-1}$).[97] Mixing carbon black with C_{60}/C_{70} did not have any beneficial effects on potential drift,[96] however, adding a fluorinated acrylic copolymer to the carbon black solid contact layer enhanced the hydrophobic character of this layer, helped prevent water layer formation, and resulted in outstanding long-term potential stability of <1 $\mu V\ h^{-1}$ over 50 h for a K^+-ISE.[116] A concern in regard to carbon black is that little is known in the open literature about the surface chemistry of commercially available versions of carbon black.

2.9. Graphene

Graphene, the building block of all of the carbon materials of interest for ISEs, but most clearly that of graphite, may appear to be another obvious choice for solid contacts (Figure 7e,f).[103,117–125] As a 2D semimetal, it is an excellent conductor of electricity along its plane and has a very high theoretical specific surface area of 2630 $m^2\ g^{-1}$. However, when deposited on a substrate, these sheets tend to form multiple layers, resulting in lower accessible surface areas. Such aggregation can be minimized by forming a reduced graphene oxide (RGO) 3D hydrogel instead, which can be prepared by mixing a graphene oxide dispersion with ethylenediamine and reducing it hydrothermally to form a monolithic porous product (experimental specific surface area 247 $m^2\ g^{-1}$, which is approximately one-tenth of the maximum theoretical value).[123] Unfortunately, because of remaining oxygen groups, the product displayed redox activity in addition to double layer capacitance, and a K^+-ISE prepared with this solid contact showed sub-Nernstian response.

The purity of graphene is highly dependent on its preparation. A common process, chemical or thermal reduction of graphene oxide to form RGO, introduces many defects into the structure, a significant number of redox-active oxygen groups may still be present, and nitrogen groups can be introduced by some reducing agents.[126] For example, after chemical reduction of graphene oxide with hydrazine, a C/O atomic ratio of 9 and a C/N ratio of 22 were achieved.[127] These heteroatom groups can result in instability of the electrode potential. The presence of acidic functional groups, such as —COOH groups, may be responsible for a small response to CO_2 that was noted for a K^+-ISE employing hydrazine-reduced graphene oxide as the solid contact.[118] A relatively large drift was observed even with high-quality graphene solid contacts, which were prepared by chemical exfoliation of intercalated graphite and which were more conductive and hydrophobic than RGO.[122] Oxygen groups can be avoided by using shear exfoliation in a fluid-dynamic reactor to produce few-layer graphene sheets from graphite powder.[103] However, even in this case, the long-term drift of ISEs prepared with this solid contact material was large (740 $\mu V\ h^{-1}$ over 15 h). In contrast, excellent potential drift values of 1.8 $\mu V\ h^{-1}$ (K^+, 27 h) and 8.8 $\mu V\ h^{-1}$ (NO_3^-, 27 h) were obtained using aminoethanethiol-functionalized RGO solid contacts that were covalently linked with gold electrodes.[124] The process of covalently linking the RGO particles to the electrode surface also enhanced the mechanical lifetime of the sensor under continuous flow conditions compared to non-anchored RGO.

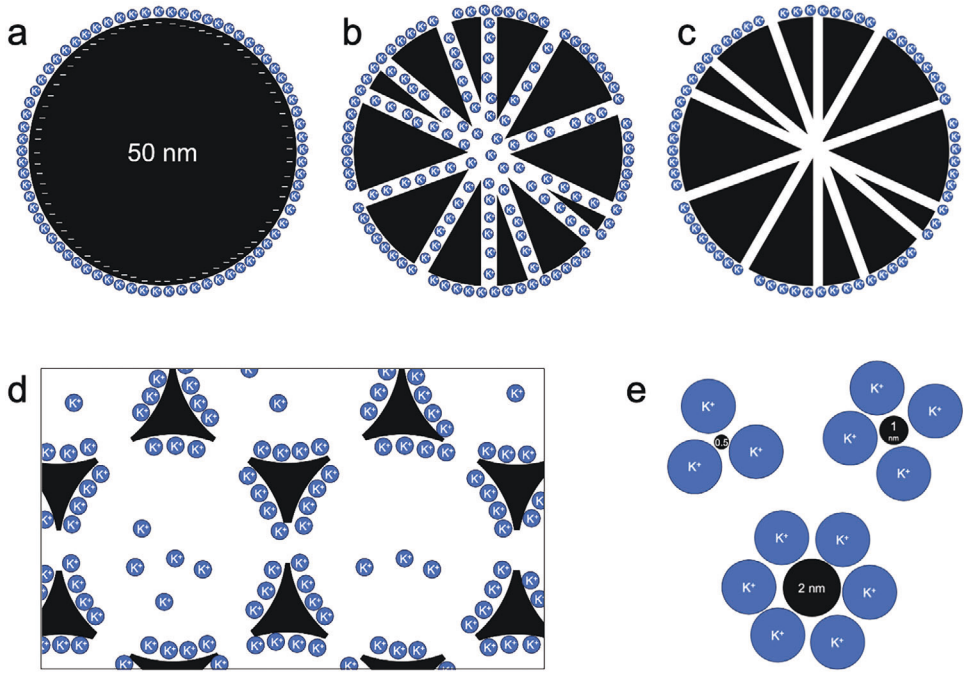

Figure 8. Schematic diagrams of K^+–valinomycin double-layer cross-sections in various nanostructured carbon substrates. a) The double layer around a 50 nm carbon nanosphere. b) The double layer of a 50 nm carbon nanosphere with 3 nm mesopores. The ionophore complexes may enter the pores, but pore blockage is possible. c) The double layer of a 50 nm carbon nanosphere with 1.8 nm micropores. Pores are not accessible to the ionophore complexes and only the external surface contributes to the double layer. d) The double layer within CIM carbon with 25 nm mesopore size. All of the surface is accessible. e) The double layer around carbon nanotubes with 0.5, 1, and 2 nm diameters. The available space for ionophore complexes is limited for the smaller diameters. The blue circles correspond to the K^+–valinomycin complexes with a diameter of 1.9 nm. The black regions correspond to the carbon phase. For clarity, negative charges in the carbon phase are shown only in (a). Within each panel, the ionophore and carbon structures are shown to scale.

3. Considerations for Choosing a Carbon-Based Solid-Contact Material

3.1. Surface Accessibility

Given the progress we have seen in all-solid-state ISEs that use carbon-based solid contacts as ion-to-electron transducers, how do we choose the best material for a specific application? In terms of sensor performance, it is not straightforward to compare all of the above systems directly, because potential drift depends on multiple parameters that are not kept constant in the literature. Even the double layer capacitance itself is influenced by multiple parameters. Importantly, the capacitance of a carbon in contact with an ISM differs from the capacitance of the bare carbon in an electrolyte solution of water or an organic solvent.[104] Factors that affect the capacitance include the polarity of the electrolyte-containing medium, the phase boundary potential at the interface to the carbon, the concentration and type of electrolytes, the pore architecture of the solid contact, the accumulation of ions at the carbon/ISM interface, and the spatial distribution of ions in the ISM.[110] Besides interfacial energy, the local curvature affects the ion concentration at the interface, so that capacitance can be different for spherical particles (carbon nanospheres/microspheres) versus spherical pores (CIM or 3DOM C) or cylindrical rods (CNTs) versus cylindrical pores (mesoporous carbon), even for identical radii.[128] The sizes of the ionophore complexes and hydrophobic ionic sites are often ignored when researchers select the highest surface area material. Accessibility of the ions in the ISM to the surface of nanoporous materials depends on pore size distributions, window openings, and pore interconnectivity. Although subnanometer pores in capacitor electrodes may contribute to anomalous capacitance,[129,130] in ISE applications, tetraphenylborate derivatives and tetraalkylammonium ions used as hydrophobic ionic sites as well as many ionophore complexes (such as valinomycin·K^+) may not be able to enter such small pores. Thus, whether small micropores should be considered irrelevant for improving ISE stability or not depends on the sizes of the ions in the ISM. In the case of micropores or small mesopores, small electrolyte ions may enter the pores when capacitance is measured without any membrane or ionophore; however, the ionophore or other components of the polymeric ISM may be selectively excluded.[110,131] For these reasons, the sizes of relevant ISM components and pore sizes should be compared when designing solid-contact ISEs (**Figure 8**). **Table 1** lists typical dimensions of ISM components. These dimensions refer to non-hydrated species, given that the ISMs are typically hydrophobic and designed to keep out water molecules. Under conditions where ions are solvated, the sizes of the solvated species should be considered. Pore size distributions can be controlled through the templating methods discussed above and can be determined from nitrogen gas sorption isotherms (see **Figure 9**). At this point, a systematic investigation of small mesopore size effects on ionophore incorporation and its influence on

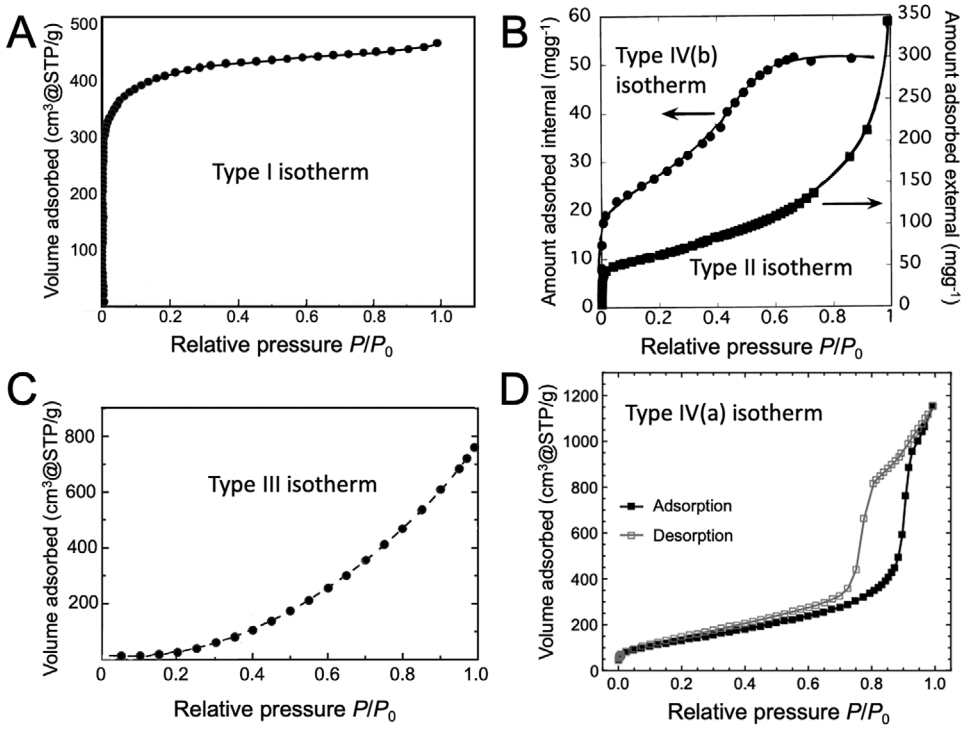

Figure 9. Representative nitrogen sorption isotherms of various carbon materials, illustrating the various types of isotherms that can be observed. A) This type I adsorption isotherm for activated carbon fibers (average pore size 1.9 nm) shows the steep rise at low relative pressure associated with micropores. Typically, no hysteresis is observed during desorption. Plotted using data from ref. [132]. B) Deconvolution of the isotherm of multiwalled carbon nanotubes with average pore widths of 4 nm, outer diameters of 10 nm, and lengths in the range of 10–100 nm. Shown are the type II isotherm for adsorption on the external nanotube surface, typical for nonporous sorbents, and the type IV(b) isotherm for adsorption to the inner nanotube surface, without hysteresis, typical for sorbents with mesopore diameters of 4 nm or less. Reprinted with permission.[133] Copyright 1998, American Chemical Society. C) Type III adsorption isotherm of macroporous C_{60} crystals, which does not show any knee at low relative pressure. This shape is typical for nonporous or macroporous solids with relatively weak adsorbent–adsorbate interactions. Adapted with permission.[114] Copyright 2013, American Chemical Society. D) Type IV(a) isotherm of CIM carbon, showing hysteresis between the adsorption and desorption processes, typical for mesoporous sorbents with pores wider than 4 nm. The rise at high relative pressure is due to the presence of textural mesopores between separate CIM carbon particles.

potential drift, using materials with similar, optimized composition is still needed, although situations such as the ones depicted in Figures 8b,d are likely to produce the highest specific capacitance values for carbon solid contacts.

Even when pores are accessible, pore order matters, and such order can be achieved using the templating methods described in Section 2 to prepare ordered mesoporous or macroporous carbon materials. In the context of supercapacitor applications, it has been concluded on the basis of molecular simulations, that carbon materials with a more ordered structure and a well-defined pore size have much higher capacitance than carbon with a disordered pore structure and a broader pore size distribution, even when both materials have the same average pore size.[136] In the ordered carbon pore structure, adsorbed ions are present in larger quantities and are more confined with more effective charge separation between anions and cations of an ionic liquid electrolyte. Disordered carbon structures contain more inaccessible sites. Among materials with low curvature (macropores and large mesopores) and high curvature (smaller mesopores, large micropores), the latter would be expected to have higher capacitance as they promote the separation of positive and negative ions.[130] In addition, if the ionophore–target ion complex has a size that differs significantly from that of the counterion, the capacitance may depend on the current direction.[110] The larger ion present in the double layer would limit the capacitance. For solid contacts with very high surface areas that are accessible to the ionophore complexes and ionic sites, the amount of ionophore or ionic site present in the ISM may become the limiting reagent, especially for thin membranes after extended use and significant charge-up of the interface.

In the case of CNTs, even though the external surface is accessible to ISM components, the number of ionophores or ionic sites that can assemble in the double layer is limited for large species around small diameter CNTs, as schematically illustrated in Figure 8e. This may limit the double-layer capacity and, in turn, the ability of the solid contact to mitigate potential drift.

3.2. Carbon Composition

In the choice of carbon for a solid contact, the material composition should also be considered. If special commercial carbon inks are used, the detailed composition and carbon morphology are not always known to the end user. Any heteroatoms present

Table 1. Critical dimensions of pores in solid contacts and components of typical ion-selective membranes.

Component	Diameter or longest dimension [nm]
Macropores	>50[a]
Mesopores	2–50[a]
Micropores	<2[a]
PVC (100 kg mol^{-1})	10[b]
Dioctyl sebacate (DOS) plasticizer	1.7[c], 2.6[d]
o-Nitrophenyl octyl ether (oNPOE) plasticizer	1.3[c], 1.7[d]
Valinomycin as K^+ complex (K^+ ionophore)	1.9[e]
o-Xylylenebis(*N*,*N*-diisobutyldithiocarbamate) (Ag^+ ionophore)	1.6[f]
Tridodecylamine (H^+ ionophore)	1.9[c], 2.7[f]
Tetrakis(pentafluorophenyl)borate (ionic site)	1.0[g], 1.3[d]

[a] IUPAC definition;[113] [b] Estimated from radius of gyration; [c] Estimated by calculating the volume per molecule from molecular weight and density, and assuming a spherical shape to calculate the diameter of that sphere; [d] Estimated using structure optimized by CrystalMaker; [e] Diameter of cross-section from published crystal structure;[134] [f] Estimated using structure optimized by CrystalMaker for the uncomplexed molecule; [g] Diameter from published DFT calculations.[135]

(oxygen, nitrogen) are prone to make the carbon more hydrophilic and more likely to support a water layer. When used in aqueous environments or in oxygen-containing atmospheres, most carbon surfaces can react with water or oxygen,[23] so that additional oxygen-containing functional groups may potentially be introduced during the use of the sensor, which could result in additional drift.

While the determination of specific functional groups in carbon materials is not always straightforward, several methods exist to determine heteroatom content in the bulk, external surface, and, for porous carbons, internal surface of carbonaceous samples.[137] Bulk elemental composition is commonly determined by a combustion analysis (the Pregl–Dumas method) for carbon, hydrogen, nitrogen, and sulfur, and, by difference, oxygen. Other bulk characterization methods that have been employed include high-resolution solid-state ^{13}C NMR, Fourier-transform IR, and Raman spectroscopy. With a focus on the outermost surface layers, X-ray photoelectron spectroscopy can provide information about the presence and amount of nitrogen and oxygen functional groups in carbon materials used for solid contacts. For accessible internal surfaces, characterization by chemical titration distinguishes between various oxygen-containing groups, including ketones, phenols, lactones, lactol, carboxylic acids, and carboxylic anhydrides. This can be supplemented by information from cyclic voltammetry (CV), which can differentiate between different surface oxygen groups. Oxygen-containing functional groups that decompose at specific temperatures to form gas-phase products may be analyzed by temperature-programmed desorption and nitrogen groups by temperature-programmed reduction. Finally, contact-angle measurements are used to evaluate surface polarity of solid contacts, which provides information about their tendency to form or avoid water layers. More details about these methods are provided in ref. [137] and citations listed therein.

3.3. Comparison of Carbon-Based Solid Contacts

Table 2 is a compilation of performance data and experimental conditions for K^+-ISEs that use different types of carbon as solid contacts. (An Excel file with a more extended table is available as Table S1, Supporting Information.) In spite of variations in experimental parameters (substrate, ISM matrix, electrode conditioning, potentiometers used, temperature control), some general conclusions about trends in potential stability can be drawn from these data. Drift is typically reported by one of two methods: either as the long-term drift, that is, the change in measured potential over time when the electrode is immersed in a solution of defined concentration (μV h^{-1} over a certain period of time); or as short-term drift when a small current is applied (typically 1 nA) in chronopotentiometric experiments (μV s^{-1}) (**Figure 10**). While the second approach involves a short experiment of a few minutes duration, the data in Table S1, Supporting Information show that this is not a reliable predictor for long-term stability. As an example, a K^+-ISE using high-quality, few-layer graphene as the solid contact produced one of the smallest reported short-term drift values (0.79 μV s^{-1} at 1 nA) but had one of the largest long-term drifts (740 μV h^{-1} over 15 h).[103] On the other hand, a K^+-ISE with CIM carbon as the solid contact exhibited the smallest long-term drift reported so far (1.3 μV h^{-1} over 70 h), while it had a similarly small short-term drift (1.0 μV s^{-1} at 1 nA).[53] This shows that the capacitance of the ISM–carbon interface is not the only relevant criterion. As discussed in this review, other important factors include the prevention of water layer formation and the stability of the ISM. While chronopotentiometrically determined capacitances provide very valuable information on the nature of the ISM–solid contact interface, for practical drift evaluations, the long-term drift is more suitable.

Measurements to determine potential drift over periods of several days or weeks should be made with good temperature control, such as by placing the entire electrochemical cell into a temperature-controlled chamber. It also requires that freshly prepared sensors be conditioned prior to such measurements by immersion into a solution containing the target ion, which leads to the uptake of water into the sensing membrane. If the sensing membrane has been prepared to contain a hydrophobic ionic site with a hydrophilic counter ion other than the target ion, conditioning also results in ion exchange, that is, target ions enter the sensing membrane, while those counter ions of the ionic sites transfer into the conditioning solution. When the cell potential is measured during conditioning, a large potential drift is typically observed early on, followed by gradual potential stabilization as the conditioning solution and the membrane reach equilibrium. As the potential drift associated with conditioning becomes smaller and smaller, it reaches a magnitude similar to the low-level long-term drift of the sensor, making it typically difficult to judge by potential measurements alone when the conditioning process is fully completed.

Proper attention must also be given to the reference electrode, as every experimentally observed potential drift is the sum of the drift contributions from the ISE and the reference electrode. Without careful usage, many commercial reference electrodes exhibit worse drifts than highly optimized solid-contact ISEs. For sample solutions that contain chloride at a constant concentration, very good results can be obtained with a AgCl-coated

Table 2. Characteristic parameters, drift, and capacitance values of selected carbon solid contacts used for K^+-ISEs. A more extended list is provided as an Excel file as Supporting Information.

Type of carbon	BET surface area[a)]	ISM matrix	Drift (short- term)	Drift (long-term)	Capacitance[b)]	Specific capacitance[b)]	Refs.
	[m^2 g^{-1}]		[µV s^{-1}]	[µV h^{-1}]	[µF]	[F g^{-1} carbon]	
3DOM C monolith, 360 nm pores, 90 nm windows	247	PVC/NPOE	1.6 (1 nA)	11.7 (70 h), 10.8 (185 h)		0.92–2.25 (cp), 3.9 (CV), 1.77 (EIS)	[21,22]
3DOM C monolith oxidized (15 min)	372	PVC/NPOE		29 (70 h)		11–68 (cp), 62 (CV)	[21]
3DOM C monolith oxidized (60 min)	467	PVC/NPOE		29 (70 h)			[21]
Untemplated RF-carbon	v. small	PVC/NPOE		1530 (70 h)			[21]
3DOM C film (interference lithography, glassy carbon)		PVC/NPOE	212 (1 nA)				[49]
3DOM C film (interference lithography, graphite)		PVC/NPOE	211 (1 nA)				[49]
CIM carbon	342	PVC/NPOE	1.0 (1 nA)	1.3 (70 h)		40.7 (cp), 31.3 (CV), 20.5 (EIS)	[53]
HOPG	v. small	PVC/NPOE		77 (96 h), 114.6 (144 h)			[22]
Glassy carbon disc	v. small	PVC/NPOE				1.09	[116]
Carbon black (Vulcan XC-72, 50 nm)	241	PVC/NPOE	19.9 (1 nA)	17.8 (172 h)			[95]
Carbon black (Printex XE-2, 30 nm)	910	PVC/NPOE	2.3–19.6 (1 nA)	9.3–15.1 (72 h)	51–429		[97]
Carbon black (Printex XE-2, 30 nm)/fluorinated polymer	1000	PVC/NPOE		<1 (50 h)	1330 (cp), 1460 (CV), 1391 (EIS)		[116]
Microporous carbon spheres (650 nm)	2006	PVC/DOS	4.8 (10 nA)	14.9 (20 h)	12 000	60	[75]
Ordered mesoporous carbon spheres (90–110 nm)	570–604	PVC/DOS	3.3 (1 nA)	28 (70 h)		17@600 °C, 53@750 °C, 11@900 °C	[74]
Microporous carbon (graphite)		PVC/DOS		150 (12 h)			[32]
Single-walled carbon nanotubes	Est.: ≈400 (144–616)	Methacrylate/acrylate	17 (1 nA), 85 (5 nA)		302 (EIS), 60 (cp)		[77]
Single-walled carbon nanotubes with octadecylamine		PVC/DOS, PVC/NPOE			50–380 (2–8 layers)		[104]
SWCNT ink on cotton yarn		PVC/DOS		<250 (short term)			[106]
SWCNT ink on rubber		PVC/DOS		400 (15 h)			[80]
Graphene (chemically reduced GO)		PVC/NPOE	12.8 (1 nA)		78.1		[117]
Graphene (chemically reduced GO)		PVC/DOS	12 (1 nA), 55 (5 nA)				[118]
Graphene (high-quality, few-layer sheets)		PVC/DOS	33 (1 nA)	180 (12 h)	34.7		[122]
Graphene (high-quality, few-layer sheets)		PVC/DOS	0.79 (1 nA)	740 (15 h)		0.21 mF cm^{-2} (CV) 1.27 mF cm^{-2} (cp)	[103]
RGO-hydrogel	247	PVC/DOS	2 (1 nA)			41 mF cm^{-2}	[123]
Thiol-functionalized RGO		PVC/DOS		1.75 (27 h)	12.4 pF		[124]

[a)] Est. refers to an estimate for a typical carbon material of that type[101] if the information was not provided in the cited reference; [b)] CV refers to data obtained by cyclic voltammetry, EIS to data obtained by electrochemical impedance spectroscopy, and cp to data obtained by chronopotentiometry.

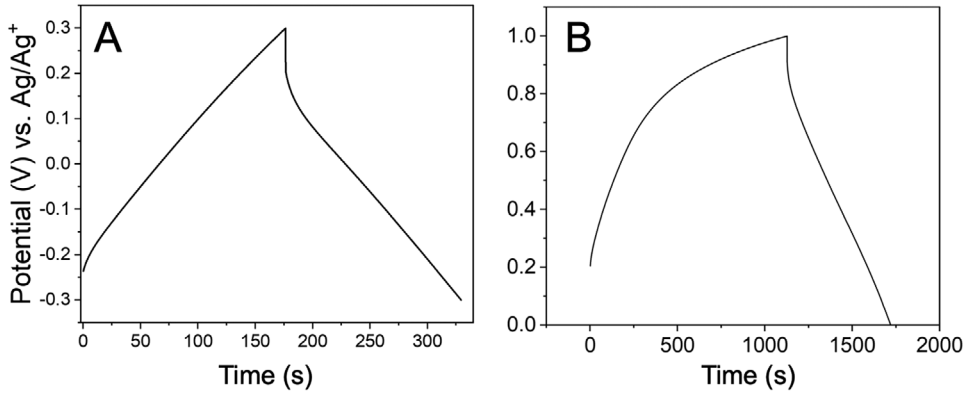

Figure 10. Determination of capacitance with chronopotentiometry, shown here for a gold electrode coated with CIM carbon immersed in acetonitrile comprising 0.1 M tetrabutylammonium perchlorate. A) Ideal experiment: The potential rises and falls linearly with time for positive and negative currents, respectively, and $C = i\,dt/dV$. The potential drops instantaneously by $2\,i\,R$ when the direction of the current is switched, where R is the cell resistance. B) Interpretation of chronopotentiograms is complicated by nonlinear dependence of potential on time, which may be caused by formation of concentration gradients, redox reactions, or potential dependence of the capacitance. Note that the chronopotentiogram shown in (A) was measured with the same electrode as (B), but with a shorter application of a smaller current (0.05 mA versus 0.1 mA), avoiding the potential from rising above 0.3 V versus Ag^+/Ag.

silver wire directly immersed into the sample, avoiding the complications associated with a liquid–liquid junction to the reference electrode. In cases where that is not possible, a free-flowing double-junction[138] or a capillary-based reference electrode[139] is recommended. While it is never possible to separate drift contributions from sensing and reference electrodes, the use of a multichannel potentiometer and measurement of the potentials of one reference electrode and the sensing electrodes of interest versus an identically prepared reference electrode are very insightful because the potential of one reference electrode versus the other reference electrode gives some sense of the stability of the reference electrode potential. Evaporation of water from the sample should be avoided to prevent an increase in the sample concentration. The input impedance of the potentiometer used should be reported. For further considerations regarding the implementation of such experiments, see ref. [8]

Among the porous carbon solid contacts in ISEs with PVC-based ISMs, the lowest long-term drift was obtained for CIM carbon with uniform, 24-nm diameter pores (1.3 μV h^{-1} over 70 h) on the surface of a gold electrode.[53] This excellent behavior may be due to a combination of multiple factors: 1) the high packing density of the pores that are fully interconnected in three dimensions and allow penetration of the ionophore as well as polymer and plasticizer; 2) the pore size, which may be close to a sweet spot for maximum infiltration with ionophore so that a high ionophore concentration in the electric double layer may be achieved; 3) the low heteroatom content in the CIM carbon that was used, which ensures hydrophobic behavior and prevents water layer formation. If one were to assume that the solid contact is the limiting factor for potential stability, further improvements might be achieved by reducing the template size slightly, perhaps to a value between 5 and 10 nm, to increase the electric double layer density while still permitting access of ionophore complexes and ionic sites into the pores. It should be noted though that the drift value increased dramatically (to 230 μV h^{-1} over 8.5 h) with a polyacrylate membrane on a PET substrate.[58] This is a reminder that drift is not only controlled by the solid contact, but that other factors also influence signal stability. For this reason, the most meaningful comparisons are those among systems using the same or similar ISM composition, which we will do here with the existing data using the PVC-based systems.

With larger pores (3DOM carbon, 12 μV h^{-1})[22] or with micro- or small mesoporous carbon spheres (15–28 μV h^{-1}),[74,75] the long-term drift is about one order of magnitude larger than for CIM carbon with PVC-based ISMs, even though the latter have higher specific surface areas than CIM carbon. This difference likely results from differences in accessibility of the ionophore complexes and ionic sites to the carbon surface. Whereas in CIM carbon, the whole surface is accessible, ionophore complexes and ionic sites may be blocked from accessing micropores and small mesopores, so that mainly the external surface of the spheres or the idealized, smooth surface of the macropore walls in 3DOM carbon is relevant.

Among nonporous carbon particles, carbon black with particle sizes of 50 nm or lower has provided some of the best long-term stability, similar to that of 3DOM carbon, especially if the carbon was decorated with platinum nanoparticles (6–18 μV h^{-1}).[95,97] With carbon nanotubes and carbon nanohorns as solid contacts, drift values exceeding 100 μV h^{-1} are typically seen, although for MWCNTs a value of 19 μV h^{-1} was reported for a Cd^{2+}-ISE.[88] While the reason for this is not yet clear, it may be related to limited surface access because of the bundling of nanotubes or to the other reasons discussed earlier. In the case of high-quality graphene-based solid contacts, the drift values are similarly high (several hundred μV h^{-1}), likely due to extensive stacking of the sheets during preparation of the solid contact films.[103,122] Potential stability improved significantly for chemically reduced graphene oxide (10 μV h^{-1}); defects introduced into the graphene sheets during the oxidation and reduction processes would inhibit stacking of sheets and maintain sufficient void space to build an electric double-layer of ionophore molecules or counterions on the large RGO surface.[119] Remarkably, one of the smallest long-term drifts reported was achieved with thiol-functionalized RGO solid contacts

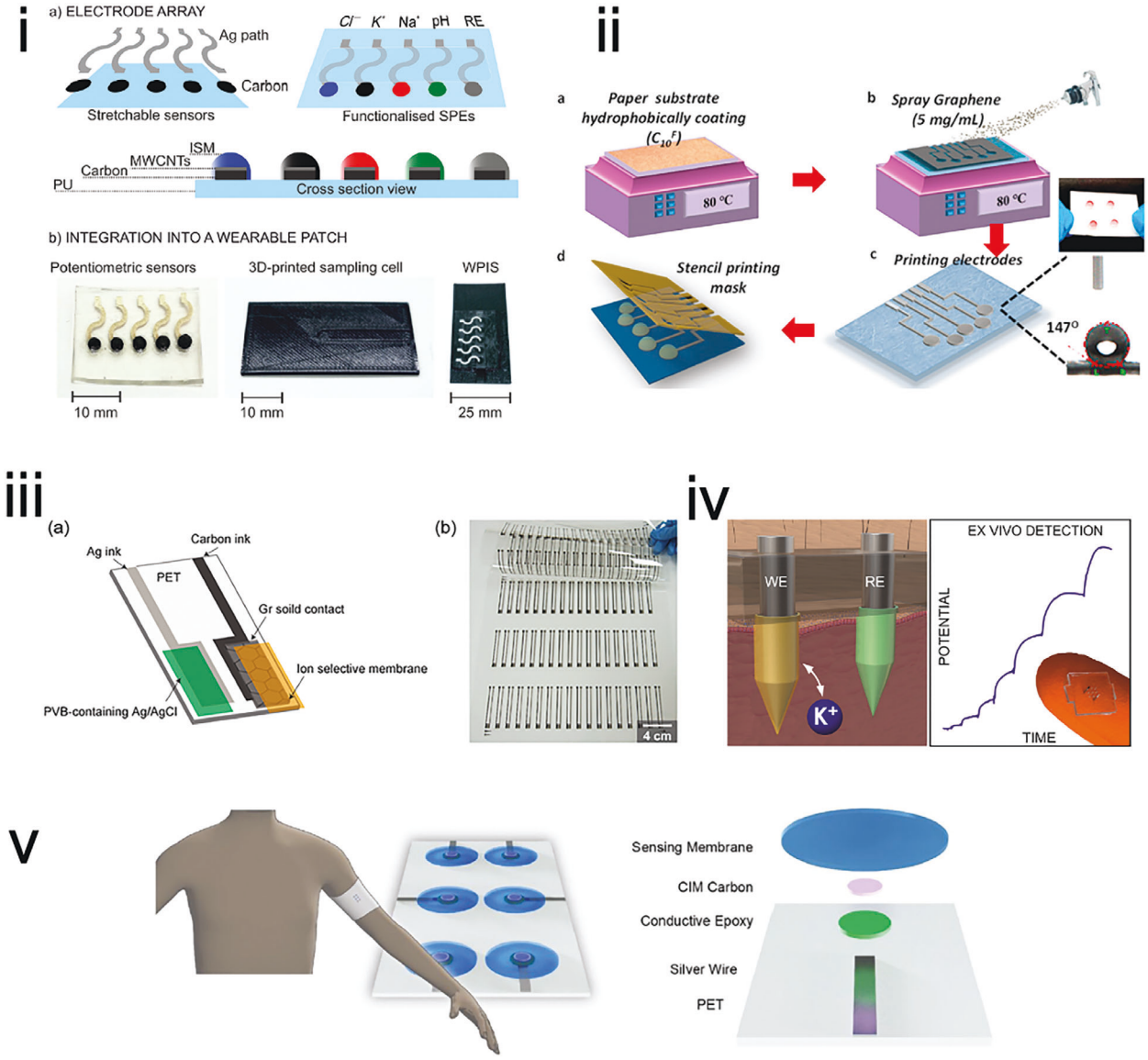

Figure 11. Advanced devices employing solid contact ISEs or reference electrodes. i-a) Electrodes in a wearable potentiometric ion sensor (WPIS) patch using MWCNTs as solid contact for on-body electrolyte monitoring in sweat. PU = polyurethane patch. SPE = stretchable potentiometric electrodes. b) Images of the electrode array, the sampling cell, and the entire wearable device. Reprinted with permission.[140] Copyright 2019, American Chemical Society. ii) Schematic representation of the fabrication of multichannel paper-based ISEs for simultaneous potentiometric sensing of K^+, Na^+, Cl^-, and pH. Graphene is used as the solid contact. Reprinted with permission.[122] Copyright 2019, Elsevier. iii-a) Scheme of screen-printed K^+-ISE sensor using graphene sheets as the solid contact. b) Photograph of the screen-printed sensor array. Reprinted with permission.[103] Copyright 2020, Elsevier. iv) Wearable all-solid-state potentiometric microneedle patch for intradermal potassium detection, using carbon nanotubes as the solid contact. Left: Schematic of the microneedle patch inserted into skin, penetrating to the dermis level of the skin for detection in the interstitial fluid. Right: Idealized calibration curve for potassium activity in skin and image of the sensor on a finger. Reprinted with permission.[86] Copyright 2019, American Chemical Society. v) Schematic of an ISE sensor array, using CIM carbon as the solid contact, supported on a flexible poly(ethylene terephthalate substrate). Reprinted with permission.[58] Copyright 2020, American Chemical Society.

($1.75\ \mu V\ h^{-1}$ over 27 h), in which covalent attachment of the thiol-RGO to the gold substrate also prevented mechanical loss under flow conditions.[124]

3.4. Other Considerations

For commercial scale manufacturing of all-solid-state ISEs, besides the performance of the electrodes, the cost, availability, and processability of the carbon solid contact become critical factors. However, it should be kept in mind that for microneedle-based and other miniaturized sensors, very small quantities of carbon are needed per sensor (less than mg quantities*), so that the material cost per sensor is small, even for more complex carbon systems. Hence, consistent quality and purity of the materials may be most critical for optimal sensor operation. Depending on the specific requirements for potential drifts in a given application, a balance may need to be found between performance, practicality

(ability to form inks, adhesion to substrate), supply chain criteria, and economics.

The obvious question arises: how much carbon is needed? This of course depends on the target drift. As an example, if a sensor for a monovalent ion has to be stable over a period of 2 weeks with a drift of less than 1.5 mV, the target drift would be 4.5 μV h^{-1} if charging of the double-layer capacitance is the only contribution to potential drift. One can use the circuit in Figure 1b as a guide to estimate the amount of carbon solid contact that would be required to achieve this value (see Equation (5)). Using CIM carbon as an example with a specific capacitance of 20 F g^{-1} and an input impedance of 100 GΩ, 0.2 mg CIM carbon would be required to reach a drift of 4.5 μV h^{-1}, ignoring other factors related to the ISM. With a potentiometer input impedance of 10 TΩ, the necessary amount would be reduced to 2 μg CIM carbon.

The thickness of the solid contact will affect total capacitance and hence long-term potential stability. Thicker ISMs require longer conditioning times but have the advantage that they contain larger total amounts of ionophore and ionic sites, which can be an advantage when ionophore and ionic sites are not covalently attached to the ISM polymer and the sensor lifetime is determined by leaching of these components into samples.

4. Recommendations for Fabrication, Characterization, and Testing of Solid-Contact Electrodes

- If synthesizing carbon materials as electron-conducting solid contacts, use a precursor with low heteroatom:carbon ratio. Even when this is done, heteroatoms may be introduced during carbon processing (templating, template extraction). Oxygen groups can then be removed to a large extent by thermal reduction in hydrogen.
- Adhesion of hydrophobic polymeric ISMs to carbon solid contacts benefits from a large interfacial area and penetration of the ISM into pores within the solid-contact layer. If stronger adhesion of the polymeric ISM to the carbon solid contact is required, covalently attach the ISM polymer to the solid contact.[33,34]
- When using commercial materials, analyze their composition. For spectroscopic elemental analysis, keep in mind whether the bulk of the material is analyzed or only the surface (e.g., XPS). It is recommended to detect potential redox activity by CV. Curvature of the potential versus time curve in chronopotentiometry traces may be an indication of redox activity but can also be the result of the build-up of ion concentration gradients in the ISM upon prolonged flow of the current, or a change in the differential capacitance as the phase boundary potential across the ISM–carbon interface is increasing in the course of the chronopotentiometry experiment.
- If using porous materials as solid contacts, it is important to know the pore size distribution and relative size of ionic species in the ISM (including the complexes of electrically neutral ionophores) to understand how much of the pore surface is accessible.
- To determine capacitance values, keep in mind that the double-layer capacitance depends on ion size, electrolyte concentration, and medium polarity. If membranes with large ionophores or ionic sites are used, capacitance values determined with the carbon material in the absence of ISM, using more concentrated solutions of much smaller electrolytes in a more polar solvent, can be misleading.
- While in principle capacitance can be determined by CV, EIS, and chronopotentiometry, CV and EIS measurements with fully assembled ISEs are hindered by the high resistance of the ISM. In the case of chronopotentiometry, one would expect little change in the capacitance values with or without the ISM. Helpful recommendations for determining accurate capacitance values of solid contact materials have recently been published.[104]
- Drifts in the calibration curves can be a sign of water layers.[13–16] It is important to watch out for such drifts in addition to carrying out the traditional water layer test. Water layer tests are often more valuable if performed after rather than before a long-term measurement.
- When measuring long-term potential drift, minimize effects arising from cell components other than the solid contact material. Control the temperature and make sure that oxygen and carbon dioxide do not affect the sensor signal. Make sure that the reference electrode does not contribute substantially to drift by testing the ISE and reference half cell independently.[8]

5. Recommendations for Reporting

- Given the importance of pore accessibility for the ionophore, ionic sites, and other ISM components, when reporting gas sorption data, besides total BET surface areas, micropore and mesopore surface areas should be reported separately and information about pore-size distribution should be included.
- Report not only capacitance but also the amount of solid contact material per sensor or specific capacitance. While for a particular solid-contact ISE drift is affected by its capacitance, different high surface-area solid contact materials can only be compared on the basis of capacitance per weight of solid contact material.
- When reporting long-term potential stability and drift, specify the solutions in which the ISEs were stored between or during measurements.
- Any ISE comprising a high surface-area solid contact should be characterized in terms of capacitance, selectivity, response slope, and limit of detection, preferably with standard deviations.[8]
- When using commercial products such as carbon materials, polymers, or ionophores, provide as many explicit characteristics as possible. Bear in mind that current versions of supplier web sites are only available to readers for a limited time, and commercial products are eventually discontinued or change characteristics over the years. Include as much pertinent information provided by suppliers. For ionophores, provide a chemical name, structure formula, or literature reference and not only a tradename.

6. Future Needs

In view of minimizing long-term drifts of ISEs, solid contacts with very high specific capacitances are desirable. However, given

the finite sizes of the relevant ions in ISMs, there is an ultimate limit to the maximum specific capacitance of a solid-contact material suitable for use in ISEs, a limit that currently available carbon materials are getting close to. Consider for example a high-performing solid contact material with a specific capacitance of 50 F g^{-1} (see Table 2). Charging this material up to −1.0 V when in contact with an ISM with the K^+ complex as the dominant cation would require formation of a double layer comprising 0.58 g of the valinomycin complex per gram of solid contact carbon. Arguably, at such a high charging state, the actual limiting factor is not capacitance per weight of carbon material but the ratio of the volume occupied by the ions and the combined volume occupied by the ions and the carbon. In the example of the valinomycin complex and 50 F g^{-1} capacitor charged to −1.0 V, this ratio is already at ≈37%, and no improvement of any type could raise this number above the maximum possible value of 100%. The use of an ever-increasing number of different carbon architectures is not going to change that.

Therefore, features other than capacitance are likely to gain increasing attention in the future. Features that have already received considerable awareness are the surface hydrophobicity, which is very important to prevent water layer formation, and the absence of heteroatoms, which can induce interference from acidic or basic species, such as carbon dioxide or ammonia, and redox-active species, such as oxygen. Another important factor is the processability of the carbon materials. For example, CNTs stand out as readily forming robust free-standing films, while other carbons require blending with a binder to prevent flaking. In view of mass manufacturing, printability, for example, by screen or inkjet printing, is also a very desirable feature, requiring small particle sizes and good dispersibility.

An aspect that requires more attention by researchers in the field is why capacitive interfaces in ISE solid contacts charge up in the first place. As it has been well-accepted for many years, when potentiometers with a relatively low input impedance are used, the major cause of charging is the input current into the potentiometer. However, in the case of high-quality potentiometers with a very high input impedance other factors may also be at play in charging or discharging capacitive interfaces. A possible cause for the charging and discharging of capacitive ISE solid contacts may also be redox reactions of either impurity components of the ISM or of the carbon material itself, but to date, little is known in regard to such phenomena. Capacitive interfaces made of carbon materials with characteristics that make them less likely to be charged up by redox reactions may be of interest in this context.

7. Conclusion

As illustrated in this Perspective, much progress has been made over the past two decades in the understanding and performance of solid-contact ISEs and reference electrodes for ion sensing. One critical component, a carbon-based solid contact, has enabled sensors that require little maintenance, are insensitive to common interferences, and can provide excellent long-term stability so that fewer calibrations are required. This greatly facilitates the development of wearable sensors, suitable for continuous measurements in on-skin or in vivo point-of-care applications (**Figure 11**). By using multiple electrodes, each with a different ionophore, the same solid-contact construct can be used for multi-target determinations in multi-channel devices. Given that several of the solid contact carbon materials can be prepared as micro- or nanoparticles, inks of these particles are suitable for assembling highly miniaturized sensors, such as microneedle or microcontact arrays. Because the amount of carbon that can be used on those microarrays is very small, if one wants to achieve the signal stability needed in continuous measurements, it is important to choose nanostructured carbon materials that provide high specific capacitance with the relevant ionophore molecules or ionic sites in the double layer. The authors hope that the criteria highlighted in this Perspective will provide helpful guidelines for future materials development for solid-contact ISEs.

Supporting Information

Supporting Information is available from the Wiley Online Library or from the author.

Acknowledgements

This work was partially supported by funding from the Industrial Partnership for Research in Interfacial and Materials Engineering (IPRIME-NMP) and from an InterS&Ections grant by the College of Science and Engineering at the University of Minnesota. Parts of this work were carried out in the University of Minnesota Characterization Facility, which receives partial support from the NSF through the MRSEC (award number DMR-2011401) and the NNCI (award number ECCS2025124) programs.

Conflict of Interest

The authors declare the following competing financial interests. A.S., P.B., and the University of Minnesota (UMN) have a patent and a patent application (U.S. patent no. 9,874,539; US2020/059979) relating to the use of CIM carbon in ion-selective and reference electrodes. The UMN and the inventors are entitled to standard royalties should licensing revenue be generated from these inventions.

Keywords

ionophore, ion-selective electrode, nanoporous carbon, nanostructured carbon, potential stability, sensors, solid contact

Received: September 20, 2023
Revised: December 5, 2023
Published online: December 17, 2023

[1] E. Bakker; E. Pretsch, in *Electroanalytical Chemistry*, Vol. *24*, (Eds: A. J. Bard, C. Zoski), CRC Press, Boca Raton, FL **2012**, pp. 1–73.
[2] G. A. Crespo, *Electrochim. Acta* **2017**, *245*, 1023.
[3] M. Cuartero, E. Bakker, *Curr. Opin. Electrochem.* **2017**, *3*, 97.
[4] P. Bühlmann, L. D. Chen, in *Supramolecular Chemistry: From Molecules to Nanomaterials*, Vol. *5* (Eds: J. W. Steed, P. A. Gale), John Wiley & Sons, New York **2012**, pp. 2539–2580.
[5] J. Hu, A. Stein, P. Bühlmann, *TrAC, Trends Anal. Chem.* **2016**, *76*, 102.
[6] Y. Shao, Y. Ying, J. Ping, *Chem. Soc. Rev.* **2020**, *49*, 4405.
[7] Y. H. Cheong, L. Ge, G. Lisak, *Anal. Chim. Acta* **2021**, *1162*, 338304.
[8] C. R. Rousseau, P. Bühlmann, *TrAC, Trends Anal. Chem.* **2021**, *140*, 116277.

[9] J. Bobacka, *Electroanalysis* **2006**, *18*, 7.
[10] D. Kaluza, A. Michalska, K. Maksymiuk, *ChemElectroChem* **2022**, *9*, 202100892.
[11] S. Amemiya, P. Bühlmann, E. Pretsch, B. Rusterholz, Y. Umezawa, *Anal. Chem.* **2000**, *72*, 1618.
[12] E. Bakker, *Talanta* **2004**, *63*, 3.
[13] M. Fibbioli, W. E. Morf, M. Badertscher, N. F. De Rooij, E. Pretsch, *Electroanalysis* **2000**, *12*, 1286.
[14] R. De Marco, J.-P. Veder, G. Clarke, A. Nelson, K. Prince, E. Pretsch, E. Bakker, *Phys. Chem. Chem. Phys.* **2008**, *10*, 73.
[15] B. Hambly, M. Guzinski, B. Pendley, E. Lindner, *Electroanalysis* **2020**, *32*, 781.
[16] J.-P. Veder, R. De Marco, G. Clarke, S. P. Jiang, K. Prince, E. Pretsch, E. Bakker, *Analyst* **2011**, *136*, 3252.
[17] J. C. Rivière, *Proc. Phys. Soc., London, Sect. B* **1957**, *70*, 676.
[18] O. Dinten, U. E. Spichiger, N. Chaniotakis, P. Gehrig, B. Rusterholz, W. E. Morf, W. Simon, *Anal. Chem.* **1991**, *63*, 596.
[19] P. Bühlmann, Y. Umezawa, S. Rondinini, A. Vertova, A. Pigliucci, L. Bertesago, *Anal. Chem.* **2000**, *72*, 1843.
[20] B. D. Spindler, K. I. Graf, X. I. N. Dong, M. Kim, X. V. Chen, P. Bühlmann, A. Stein, *Anal. Chem.* **2023**, *95*, 12419.
[21] M. A. Fierke, C.-Z. Lai, P. Bühlmann, A. Stein, *Anal. Chem.* **2010**, *82*, 680.
[22] C.-Z. Lai, M. A. Fierke, A. Stein, P. Bühlmann, *Anal. Chem.* **2007**, *79*, 4621.
[23] R. L. Mccreery, *Chem. Rev.* **2008**, *108*, 2646.
[24] C. A. Klein, *Rev. Mod. Phys.* **1962**, *34*, 56.
[25] J. D. Arregui-Mena, P. D. Edmondson, A. A. Campbell, Y. Katoh, *J. Nucl. Mater.* **2018**, *511*, 164.
[26] M. Wissler, *J. Power Sources* **2006**, *156*, 142.
[27] J. Ruzicka, J. C. Tjell, *Anal. Chim. Acta* **1970**, *51*, 1.
[28] J. Ruzicka, K. Rald, *Anal. Chim. Acta* **1971**, *53*, 1.
[29] J. Ruzicka, C. G. Lamm, J. C. Tjell, *Anal. Chim. Acta* **1972**, *62*, 15.
[30] M. Vamvakaki, N. A. Chaniotakis, *Anal. Chim. Acta* **1996**, *320*, 53.
[31] N. A. Chaniotakis, S. J. West, US5840168A, **1998**.
[32] A. W. Weber, G. D. O'neil, S. P. Kounaves, *Anal. Chem.* **2017**, *89*, 4803.
[33] K. R. Choi, X. V. Chen, J. Hu, P. Bühlmann, *Anal. Chem.* **2021**, *93*, 16899.
[34] K. R. Choi, B. K. Troudt, P. Bühlmann, *Angew. Chem., Int. Ed.* **2023**, *62*, 202304674.
[35] Y. Chipangura, P. Bühlmann, A. Stein, unpublished, **2023**.
[36] V. Kasi, S. Sedaghat, A. M. Alcaraz, M. K. Maruthamuthu, U. Heredia-Rivera, S. Nejati, J. Nguyen, R. Rahimi, *ACS Appl. Mater. Interfaces* **2022**, *14*, 9697.
[37] S. Sedaghat, V. Kasi, S. Nejati, A. Krishnakumar, R. Rahimi, *J. Mater. Chem. C* **2022**, *10*, 10562.
[38] V. Uskokovic, *Carbon Trends* **2021**, *5*, 100116.
[39] M. Fouskaki, N. A. Chaniotakis, *Anal. Chem.* **2005**, *77*, 1780.
[40] C.-Z. Lai, M. M. Joyer, M. A. Fierke, N. D. Petkovich, A. Stein, P. Bühlmann, *J. Solid State Electrochem.* **2009**, *13*, 123.
[41] C.-Z. Lai, M. A. Fierke, R. C. Da Costa, J. A. Gladysz, A. Stein, P. Bühlmann, *Anal. Chem.* **2010**, *82*, 7634.
[42] T. Zhang, C.-Z. Lai, M. A. Fierke, A. Stein, P. Bühlmann, *Anal. Chem.* **2012**, *84*, 7771.
[43] L. D. Chen, C.-Z. Lai, L. P. Granda, M. A. Fierke, D. Mandal, A. Stein, J. A. Gladysz, P. Bühlmann, *Anal. Chem.* **2013**, *85*, 7471.
[44] A. A. Zakhidov, R. H. Baughman, Z. Iqbal, C. Cui, I. Khayrullin, S. O. Dantas, J. Marti, V. G. Ralchenko, *Science* **1998**, *282*, 897.
[45] K. T. Lee, J. C. Lytle, N. S. Ergang, S. M. Oh, A. Stein, *Adv. Funct. Mater.* **2005**, *15*, 547.
[46] Z. Wang, N. S. Ergang, M. A. Al-Daous, A. Stein, *Chem. Mater.* **2005**, *17*, 6805.
[47] Z. Wang, F. Li, N. S. Ergang, A. Stein, *Chem. Mater.* **2006**, *18*, 5543.
[48] Y. Wang, M. Wang, X. Ge, *Langmuir* **2014**, *30*, 10804.
[49] P. R. Miller, X. Xiao, I. Brener, D. B Burckel, R. Narayan, R. Polsky, *Adv. Healthcare Mater.* **2014**, *3*, 876.
[50] T. Sokalski, A. Ceresa, M. Fibbioli, T. Zwickl, E. Bakker, E. Pretsch, *Anal. Chem.* **1999**, *71*, 1210.
[51] M. Püntener, M. Fibbioli, E. Bakker, E. Pretsch, *Electroanalysis* **2002**, *14*, 1329.
[52] X. I. N. Dong, B. D. Spindler, M. Kim, A. Stein, P. Bühlmann, *ACS Sens.* **2023**, *8*, 1774.
[53] J. Hu, X. U. Zou, A. Stein, P. Bühlmann, *Anal. Chem.* **2014**, *86*, 7111.
[54] Y. Fang, D. Gu, Y. Zou, Z. Wu, F. Li, R. Che, Y. Deng, B. Tu, D. Zhao, *Angew. Chem., Int. Ed.* **2010**, *49*, 7987.
[55] A. Vu, X. Li, J. Phillips, A. Han, W. H. Smyrl, P. Bühlmann, A. Stein, *Chem. Mater.* **2013**, *25*, 4137.
[56] J. Hu, K. T. Ho, X. U. Zou, W. H. Smyrl, A. Stein, P. Bühlmann, *Anal. Chem.* **2015**, *87*, 2981.
[57] J. Hu, W. Zhao, P. Bühlmann, A. Stein, *ACS Appl. Mater. Interfaces* **2018**, *1*, 293.
[58] E. L. Anderson, S. A. Chopade, B. Spindler, A. Stein, T. P. Lodge, M. A. Hillmyer, P. Bühlmann, *Anal. Chem.* **2020**, *92*, 7621.
[59] J. Hu, P. Bühlmann, A. Stein, US9874539B2, **2018**.
[60] X. Chen, A. Stein, P. Bühlmann, US111573194B2, **2023**.
[61] Z. Li, M. Jaroniec, *J. Am. Chem. Soc.* **2001**, *123*, 9208.
[62] Z. Li, M. Jaroniec, Y.-J. Lee, L. R. Radovic, *Chem. Commun.* **2002**, 1346.
[63] Z. Li, M. Jaroniec, *J. Phys. Chem. B* **2004**, *108*, 824.
[64] Z. Li, M. Jaroniec, *Anal. Chem.* **2004**, *76*, 5479.
[65] Z. Li, M. Jaroniec, *Chem. Mater.* **2003**, *15*, 1327.
[66] B. Fang, J. H. Kim, J.-S. Yu, *Electrochem. Commun.* **2008**, *10*, 659.
[67] B. Fang, M. Kim, S. Hwang, J.-S. Yu, *Carbon* **2008**, *46*, 876.
[68] K. Pei, D. Banham, F. Feng, T. Fuerstenhaupt, S. Ye, V. Birss, *Electrochem. Commun.* **2010**, *12*, 1666.
[69] X. V. Chen, A. Stein, P. Bühlmann, *ACS Sens.* **2020**, *5*, 1717.
[70] E. L. Anderson, S. A. Chopade, B. Spindler, A. Stein, T. P. Lodge, M. A. Hillmyer, P. Bühlmann, *Anal. Chem.* **2020**, *92*, 7621.
[71] X. Li, D. Banham, F. Feng, F. Forouzandeh, S. Ye, D. Y. Kwok, V. Birss, *Carbon* **2015**, *87*, 44.
[72] X. Li, F. Forouzandeh, A. J. Kakanat, F. Feng, D. W. H. Banhan, S. Ye, D. Y. Kwok, V. Birss, *ACS Appl. Mater. Interfaces* **2018**, *10*, 2130.
[73] T. Yin, T. Han, C. Li, W. Qin, J. Bobacka, *Anal. Chim. Acta* **2020**, *1101*, 50.
[74] Z. Jiang, X. Xi, S. Qiu, D. Wu, W. Tang, X. Guo, Y. Su, R. Liu, *J. Mater. Sci.* **2019**, *54*, 13674.
[75] J. Ye, F. Li, S. Gan, Y. Jiang, Q. An, Q. Zhang, L. Niu, *Electrochem. Commun.* **2015**, *50*, 60.
[76] Y. Kumar, G. P. Pandey, S. A. Hashmi, *J. Phys. Chem. C* **2012**, *116*, 26118.
[77] G. A. Crespo, S. Macho, F. X Rius, *Anal. Chem.* **2008**, *80*, 1316.
[78] G. A. Crespo, S. Macho, J. Bobacka, F. X Rius, *Anal. Chem.* **2009**, *81*, 676.
[79] P. Yanez-Sedeno, J. Riu, J. M. Pingarron, F. X. Rius, *TrAC, Trends Anal. Chem.* **2010**, *29*, 939.
[80] M. Cuartero, J. S. Del Río, P. Blondeau, J. A. Ortuño, F. X. Rius, F. J. Andrade, *Anal. Chim. Acta* **2014**, *827*, 95.
[81] G. A. Crespo, D. Gugsa, S. Macho, F. X. Rius, *Anal. Bioanal. Chem.* **2009**, *395*, 2371.
[82] M. Cuartero, J. Bishop, R. Walker, R. G. Acres, E. Bakker, R. De Marco, G. A. Crespo, *Chem. Commun.* **2016**, *52*, 9703.
[83] S. S. M. Hassan, A. G. Eldin, A. E.-G. E. Amr, M. A. Al-Omar, A. H. Kamel, N. M. Khalifa, *Sensors* **2019**, *19*, 3891.
[84] G. Kerric, E. J. Parra, G. A. Crespo, F. Xavier Rius, P. Blondeau, *J. Mater. Chem.* **2012**, *22*, 16611.
[85] C. Ocana, N. Abramova, A. Bratov, T. Lindfors, J. Bobacka, *Talanta* **2018**, *186*, 279.

[86] M. Parrilla, M. Cuartero, S. Padrell Sánchez, M. Rajabi, N. Roxhed, F. Niklaus, G. A. Crespo, *Anal. Chem.* **2019**, *91*, 1578.
[87] D. Yuan, A. H. C. Anthis, M. Ghahraman Afshar, N. Pankratova, M. Cuartero, G. A. Crespo, E. Bakker, *Anal. Chem.* **2015**, *87*, 8640.
[88] C. Wardak, *Sens. Actuators, B* **2015**, *209*, 131.
[89] Y. Liu, Y. Liu, R. Yan, Y. Gao, P. Wang, *Electrochim. Acta* **2020**, *331*, 135370.
[90] M. Samardzic, M. Persic, A. Széchenyi, M. Jozanovic, I. Pukles, M. Budetic, *Sensors* **2023**, *23*, 2641.
[91] C. Jiang, Y. Yao, Y. Cai, J. Ping, *Sens. Actuators, B* **2019**, *283*, 284.
[92] M. Fibbioli, O. Enger, F. Diederich, E. Pretsch, K. Bandyopadhyay, S.-G. Liu, L. Echegoyen, P. Bühlmann, *Chem. Commun.* **2000**, 339.
[93] M. Fibbioli, K. Bandyopadhyay, S.-G. Liu, L. Echegoyen, O. Enger, F. Diederich, D. Gingery, P. Bühlmann, H. Persson, U. W. Suter, E. Pretsch, *Chem. Mater.* **2002**, *14*, 1721.
[94] M. Fouskaki, N. Chaniotakis, *Analyst* **2008**, *133*, 1072.
[95] B. Paczosa-Bator, L. Cabaj, R. Piech, K. Skupien, *Anal. Chem.* **2013**, *85*, 10255.
[96] N. M. Ivanova, I. V. Podeshvo, M. Y. Goikhman, A. V. Yakimanskii, K. N. Mikhelson, *Sens. Actuators, B* **2013**, *186*, 589.
[97] B. Paczosa-Bator, *Talanta* **2012**, *93*, 424.
[98] US_Research_Nanomaterials. Research Grade Large Inner Diameter Thin-Walled MWCNTs, https://www.us-nano.com/inc/sdetail/313 (accessed: July 2023).
[99] Y. Matsuda, J. Tahir-Kheli, W. A. Goddard, *J. Phys. Chem. Lett.* **2010**, *1*, 2946.
[100] M. J. O'connell, S. M. Bachilo, C. B. Huffman, V. C. Moore, M. S. Strano, E. H. Haroz, K. L. Rialon, P. J. Boul, W. H. Noon, C. Kittrell, J. Ma, R. H. Hauge, R. B. Weisman, R. E. Smalley, *Science* **2002**, *297*, 593.
[101] M. E. Birch, T. A. Ruda-Eberenz, M. Chai, R. Andrews, R. L. Hatfield, *Ann. Occup. Hyg.* **2013**, *57*, 1148.
[102] J. Zhu, X. Li, Y. Qin, Y. Zhang, *Sens. Actuators, B* **2010**, *148*, 166.
[103] H. J. Park, J.-M. Jeong, J. H. Yoon, S. G. Son, Y. K. Kim, D. H. Kim, K. G. Lee, B. G. Choi, *J. Colloid Interface Sci.* **2020**, *560*, 817.
[104] E. Zdrachek, E. Bakker, *Microchim. Acta* **2021**, *188*, 149.
[105] M. Novell, M. Parrilla, G. A. Crespo, F. X Rius, F. J. Andrade, *Anal. Chem.* **2012**, *84*, 4695.
[106] T. Guinovart, M. Parrilla, G. A. Crespo, F. X. Rius, F. J. Andrade, *Analyst* **2013**, *138*, 5208.
[107] Á. Molinero-Fernández, A. Casanova, Q. Wang, M. Cuartero, G. A. Crespo, *ACS Sens.* **2023**, *8*, 158.
[108] J. J. García-Guzmán, C. Pérez-Ràfols, M. Cuartero, G. A. Crespo, *ACS Sens.* **2021**, *6*, 1129.
[109] C. Punckt, M. A. Pope, J. Liu, Y. Lin, I. A. Aksay, *Electroanalysis* **2010**, *22*, 2834.
[110] C. R. Rousseau, Ph.D. Thesis, University of Minnesota, Twin Cities **2022**.
[111] M. Knupfer, *Surf. Sci. Rep.* **2001**, *42*, 1.
[112] J. Li, T. Yin, W. Qin, *Anal. Chim. Acta* **2015**, *876*, 49.
[113] M. Thommes, K. Kaneko, A. V. Neimark, J. P. Olivier, F. Rodriguez-Reinoso, J. Rouquerol, K. S. W. Sing, *Pure Appl. Chem.* **2015**, *87*, 1051.
[114] L. K. Shrestha, Y. Yamauchi, J. P. Hill, K. Miyazawa, K. Ariga, *J. Am. Chem. Soc.* **2013**, *135*, 586.
[115] M. Carmo, A. R. Dos Santos, J. G. R. Poco, M. Linardi, *J. Power Sources* **2007**, *173*, 860.
[116] B. Paczosa-Bator, *Carbon* **2015**, *95*, 879.
[117] J. Ping, Y. Wang, J. Wu, Y. Ying, *Electrochem. Commun.* **2011**, *13*, 1529.
[118] F. Li, J. Ye, M. Zhou, S. Gan, Q. Zhang, D. Han, L. Niu, *Analyst* **2012**, *137*, 618.
[119] R. Hernández, J. Riu, J. Bobacka, C. Vallés, P. Jiménez, A. M. Benito, W. K. Maser, F. X Rius, *J. Phys. Chem. C* **2012**, *116*, 22570.
[120] E. Jaworska, W. Lewandowski, J. Mieczkowski, K. Maksymiuk, A. Michalska, *Analyst* **2013**, *138*, 2363.
[121] Z. A. Boeva, T. Lindfors, *Sens. Actuators, B* **2016**, *224*, 624.
[122] Q. An, S. Gan, J. Xu, Y. Bao, T. Wu, H. Kong, L. Zhong, Y. Ma, Z. Song, L. Niu, *Electrochem. Commun.* **2019**, *107*, 106553.
[123] J. H. Yoon, H. J. Park, S. H. Park, K. G. Lee, B. G. Choi, *Carbon Lett.* **2020**, *30*, 73.
[124] Y. Liu, Y. Liu, Z. Meng, Y. Qin, D. Jiang, K. Xi, P. Wang, *Talanta* **2020**, *208*, 120374.
[125] A. M. Michael, A. M. Mahmoud, N. M. Fahmy, *BMC Chem.* **2023**, *17*, 27.
[126] H. Kim, A. A. Abdala, C. Macosko, *Macromolecules* **2010**, *43*, 6515.
[127] S. Stankovich, R. D. Piner, X. Chen, N. Wu, S. T. Nguyen, R. S. Ruoff, *J. Mater. Chem.* **2006**, *16*, 155.
[128] F. Yang, *Phys. Lett. A* **2019**, *383*, 2353.
[129] C. Largeot, C. Portet, J. Chmiola, P.-L. Taberna, Y. Gogotsi, P. Simon, *J. Am. Chem. Soc.* **2008**, *130*, 2730.
[130] J. Wu, *Chem. Rev.* **2022**, *122*, 10821.
[131] J. N. Neal, D. J. Wesolowski, D. Henderson, J. Wu, *J. Chem. Phys.* **2017**, *146*, 174701.
[132] L. Zhang, L.-Y. Tu, Y. Liang, Q. Chen, Z.-S. Li, C.-H. Li, Z.-H. Wang, W. Li, *RSC Adv.* **2018**, *8*, 42280.
[133] S. Inoue, N. Ichikuni, T. Suzuki, T. Uematsu, K. Kaneko, *J. Phys. Chem. B* **1998**, *102*, 4689.
[134] T. Wyttenbach, J. J. Batka, J. Gidden, M. T. Bowers, *Int. J. Mass Spectrom.* **1999**, *193*, 143.
[135] J. Langmaier, S. Zális, Z. Samec, V. Bovtun, M. Kempa, *Electrochim. Acta* **2013**, *87*, 591.
[136] E. H. Lahrar, P. Simon, C. Merlet, *J. Chem. Phys.* **2021**, *155*, 184703.
[137] A. Stein, Z. Wang, M. A. Fierke, *Adv. Mater.* **2009**, *21*, 265.
[138] R. E. Dohner, D. Wegmann, W. E. Morf, W. Simon, *Anal. Chem.* **1986**, *58*, 2585.
[139] E. L. Anderson, B. K. Troudt, P. Bühlmann, *ACS Sens.* **2021**, *6*, 2211.
[140] M. Parrilla, I. Ortiz-Gómez, R. Cánovas, A. Salinas-Castillo, M. Cuartero, G. A. Crespo, *Anal. Chem.* **2019**, *91*, 8644.

Yevedzo Chipangura received her B.S. in Chemistry and Mathematics from The College of St Scholastica in Duluth, Minnesota. She is currently a Ph.D. candidate in Prof. Andreas Stein's group at the University of Minnesota Twin Cities, Department of Chemistry. Her research interests are in the development of nanostructured and nanoporous materials for electrochemical applications, such as energy storage and chemical sensing.

Brian Spindler received his B.S. degree from the Department of Chemistry and Biochemistry at the University of Wisconsin Milwaukee. He is currently a Ph.D. candidate in Prof. Stein's group in the Department of Chemistry at the University of Minnesota. His research focuses on the design of biocompatible ion-selective sensors.

Philippe Bühlmann obtained a Ph.D. degree from the Swiss Federal Institute of Technology Zürich. After 8 years at the University of Tokyo, he joined in 2000, the Department of Chemistry at the University of Minnesota Twin Cities, where he is now a College of Science and Engineering Distinguished Professor. His research group develops receptor-based electroanalytical sensors, with a focus on the synthesis and efficient use of highly selective ionophores, biofouling resistant materials, as well as advanced polymers and nanostructured materials for reliable long-term ion monitoring with minimal needs for (re)calibration.

Andreas Stein obtained his Ph.D. in Chemistry from the University of Toronto and is currently a Distinguished McKnight University Professor in the Department of Chemistry at the University of Minnesota. His research interests are in the field of materials chemistry, in particular porous materials and nanocomposites with control over the architecture and composition of the materials at multiple length scales through templating methods. His research group has applied these materials to a wide range of applications, including energy storage and conversion, sorption, sensing, and structural materials. He is also a co-editor of the six-volume "Handbook of Solid-State Chemistry."